TAMPEREEN TEKNILLINEN YLIOPISTO
TAMPERE UNIVERSITY OF TECHNOLOGY

WENBO WANG

INDOOR MOBILITY MODELS FOR WIRELESS POSITIONING

Master of Science thesis

Examiners:
Associate Prof. Elena Simona Lohan
Adjunct Prof. Oana Cramariuc
Examiners and topic approved by the Faculty Council of the Faculty of Computing and Electrical Engineering on 4th February 2015

ABSTRACT

WENBO WANG: INDOOR MOBILITY MODELS FOR WIRELESS POSITIONING
Tampere University of Technology
Master of Science thesis, 60 pages, 11 Appendix pages
May 2015
Master's Degree Programme in Electrical Engineering
Major: Wireless Communications Circuits and Systems
Examiners: Associate Prof. Elena Simona Lohan and Adjunct Prof. Oana Cramariuc
Keywords: Indoor positioning, mobility model, fingerprint method, Bayesian estimation

Indoor positioning technology has become increasingly popular in both business and research worlds. Several technologies have been developed so far and some of them are in commercial use now. However, due to personal privacy issues and the complexity of indoor environment, the data regarding the human mobility patterns are insufficient. The study of synthetic human mobility models is an important issue, which is expected to shed new light into a myriad of Location Based Services and location-aware communications. Finding and testing synthetic models about human mobility is an important step ahead and this constitutes the main focus of this thesis. In addition, we also address the issue of indoor positioning via WiFi received signal strength under various mobility patterns, generated synthetically through a simulator built within this thesis.

The thesis starts with a review of four popular synthetic human mobility models which is followed by presenting a new model proposed in this work and denoted as Hybrid Model. Based on the suitability of the models for indoor positioning, the Random Direction Mobility Model and the newly proposed Hybrid models were chosen for further testing as human mobility models with WiFi-based fingerprinting. We show in detail the indoor scenarios characterization and accordingly we present the classical path loss model. Then, an indoor positioning simulator including mobility models is built and an alternative method of evaluating Access Points (APs) deployment is introduced. In order to explore the positioning accuracy of the above two models, a fingerprinting algorithm with Bayesian combining is applied. The results are shown in terms of Root Mean Square Error (RMSE) distance error. Finally we conclude that a Hybrid Model has a better positioning accuracy than a Random Direction Mobility Model and that neither of the two models is essentially affected by the velocity range or by the variation of the starting point. We also show how the noise variance affects the positioning results.

PREFACE

This Master of Science Thesis has been carried out at the Department of Electronics and Communication Engineering in Tampere University of Technology (TUT), Tampere, Finland during October 2013 and April 2015.

Firstly and most importantly, I would like to deeply thank my supervisor Dr. Elena-Simona Lohan, because she kindly gave me the topic near the beginning of my master study. I have been under her supervision and instruction for almost two years. At first, I did not even know the meaning of 'thesis' and made a joke. But thank to her patience, I got this topic and kept working on it for this long time.

Secondly, I would like to thank my examiner Dr. Oana Cramariuc, her appearance in my thesis presentation means a lot. Her support gave me confidence and persistence.

Thirdly, I would like to thank people I know and people I do not know here, they are peaceful, friendly, helpful and patient, if I dare to list all these good qualities they have, I am afraid it will cost me a whole day long.

Finally, I would like to take a deep bow to my parents, they do not know English, they do not know anything about my work, but their support is unconditional and eternal. I love you, my father and my mother. You are the best!

Tampere, 18.05.2015

Wenbo Wang

TABLE OF CONTENTS

LIST OF FIGURES

LIST OF TABLES

LIST OF ABBREVIATIONS AND SYMBOLS

AP	Access Point
AOA	Angle Of Arrival
GNSS	Global Navigation Satellite System
IR	Infrared Radiation
RFID	Radio Frequency Identification
RMSE	Root Mean Square Error
RSSI	Received Signal Strength Indication
TDOA	Time Difference Of Arrival
TOA	Time Of Arrival
UWB	Ultra-wide Bandwidth
WLAN	Wireless Local Area Network

(x_n, y_n, z_n)	coordinate of track point
x_{ap}, y_{ap}, z_{ap}	coordinate of the ap-th AP
v_n	velocity
θ_n	angle
Δt	moving duration
τ	resolution time interval
Δd	displacement
$P_{T_{ap}}$	transmitted power
n_{ap}	path loss coefficient
$\eta_{i,ap}$	shadowing and fading
$\xi_{i,ap}$	floor loss
$P_{i,ap}$	received power of fingerprints
R_{ap}	received power of track points
σ_{ap}^2	shadowing variance
r_{ap}	radiation radius of an AP
L_i	likelihood of estimation
$(\hat{x}, \hat{y}, \hat{z})$	value of estimation

1. INTRODUCTION

1.1 Motivation

Over the last decade, the development of Global Navigation Satellite System (GNSS) based technology has been changing the world profoundly. With this innovation, many location-related services and projects were born, which reformed and are still reforming our very lives day by day. Moreover, now when this thesis is being written, enormous location-based smart phone applications and wearable equipment are given birth to. However, the GNSS only works outstandingly under outdoor scenarios, while in indoor situation it is nearly blind because of the complexity of buildings (i.e., shadowing and multi-path effect [9]), signal physical characteristics (i.e., the significant attenuation of microwave through roofs and walls [9]) etc. In addition, as a matter of fact, a large number of people spend most of the hours in a day staying inside a building, for example, the office hours. Therefore, the concept of indoor positioning is an active field of research with multiple foreseen applications.

To start with, by reviewing the literature, some of current indoor positioning technologies and systems are presented below with a brief introduction:

1. **Microsoft RADAR** [8]: A tracking system which uses Wireless Local Area Network (WLAN) Received Signal Strength Indication (RSSI) technology. It has low accuracy level (around 4 m) and low reliability [18];

2. **Ekahau** [2]: A system that can simultaneously tracks thousands of devices using WLAN RSSI technology. It has relative high accuracy level (up to 1 m) and low cost [18];

3. **Horus** [44]: A system which uses WLAN RSSI technology with the *Bayesian* estimation method. It has relative high accuracy level (below 2.1 m) and fair complexity [27];

4. **COMPASS** [24]: A system which uses both WLAN and digital compass to provide position information. It has relative high accuracy level (1-2 m) and

inexpensive cost [18];

5. **Ubisense** [4]: A system which uses tags attached on mobiles to transmit Ultra-wide bandwidth (UWB) signals to network and performs localization based on the angle of arrival (AOA) or time difference of arrival (TDOA) method. It has excellent accuracy level (below 0.3 m) but high cost [27];

6. **Easy Living** [11]: A system which uses vision-based technology for localization. It has inexpensive cost but low reliability due to dynamic changing environment and complex image processing. Besides, the available accuracy is uncertain [18];

7. **Firefly** [22]: An Infrared Radiation -based (IR) motion tracking system. It has excellent accuracy level (below 0.003 m) but high cost and wearing-comfort problems [18];

8. **SpotON** [21]: A well-known Radio Frequency Identification RFID-based solution with Ad Hoc manner. It has flexible accuracy level (depending on the cluster size), low cost and medium complexity [27];

9. **Active Bat** [1]: A system which uses ultrasonic technology as transmitted medium to locate users. It has excellent accuracy level (around 0.03 m) and high cost [18].

Among these solutions, WLAN-based methods have acceptable accuracy, relatively low cost, fair complexity and medium reliability. Besides, the continuous growing number of personal wireless equipment gives us an opportunity of realizing indoor positioning through current wireless technologies (i.e., cellular and WLAN signals [30, 38]). Thus, the WLAN-based RSSI method is now a feasible and promising option for large-scale positioning.

In indoor scenarios, movement of wireless devices has significant impact on the wireless environment. To reveal human mobility patterns could help the research and improve positioning methods, and help to optimize the network as well. Conventionally, human mobility models are divided into two categories: *trace-based models* and *synthetic models* [37]. Trace-based models are statistical models using real data from real life. They guarantee genuine description of human trajectory. Unlike trace-based models, synthetic models are artificial models which start from some empirical parameter assumptions. However, one one hand, collecting trace data often poses privacy issues and ethical problems, and in most countries it is illegal to touch this line unless the express consent of the tracked users is given; on the other

hand, it is not easy to sample the data in order to meet the indoor positioning accuracy requirement. In this sense, synthetic models are more suitable for large-scale indoor positioning properties study. Therefore, this thesis work is mainly related to synthetic models such as building models, comparisons among models, test of selected models with a certain fingerprint algorithm etc.

1.2 Author contribution

In this work, the following contribution has been made by the author:

1. Review of the solutions for indoor positioning scenario where GNSS is not available;
2. Study and exploration of properties of various contextual models, such as supersonic sound positioning system and vision-based positioning system;
3. Implementation of four of the most popular synthetic models currently existing in the literature. In this step, some limitations were added to the models so that some models are more realistic;
4. Comparison of the introduced models from different angles and analysis of their pros and cons;
5. Proposing a novel model which attempts to mimic the real indoor human movement patterns, the Hybrid Mobility model;
6. General description of the indoor environment and simulation-based modeling of a indoor channel, including path losses and shadowing.
7. Testing different mobility models under indoor wireless circumstance using the fingerprint algorithm and Bayesian estimation;
8. Drawing conclusions on the results and presenting an outlook on future development.

In the end of thesis work, the author submitted one publication as the first author, namely: Wenbo Wang, Pedro Figueiredo e Silva and Elena Simona Lohan, 'Investigations on mobility models and their impact on indoor positioning', submitted to MOBIQUITOUS 2015 (JUFO 1 level conference). The content of this publication is related to investigation of current human mobility models and explain in detail the reason of proposing the Hybrid Model, and using fingerprinting algorithm to test the proposed Hybrid Model and other models found in the literature.

1.3 Thesis organization

There are nine chapters in this thesis, details are as follow:

Chapter 2: introduces the concept of contextual model, and explores the properties of it. From a big picture point of view, this chapter describes the main thesis idea and which movement properties can be used to model, which natural properties can be used as a medium to model the trajectory of a moving object.

Chapter 3: introduces the current four popular synthetic models namely Random Walk Mobility Model, Random Waypoint Mobility Model, Random Direction Mobility Model and Boundless Simulation Area Mobility Model. Finally we propose a novel indoor human mobility model, namely the Hybrid Model.

Chapter 4: In this chapter, the characterization of indoor scenarios is presented. The assumption of human mobility and classical path loss model are introduced. In the end, the processes of fingerprinting and estimation method are given.

Chapter 5: Matlab simulator is described in detail. In this chapter we also give an alternative method of evaluating the APs deployment inside a building. Afterwards, the methodology of forming fingerprint database and the track database is introduced.

Chapter 6: The simulation-based results are shown. The main performance criteria is the distance root mean square error.

Chapter 7: discusses the tradeoffs when designing a positioning algorithm under certain mobility model parameters.

Chapter 8: presents some innovative ideas on estimating the angle and velocity based on RSS information. This work is only in an incipient phase and open issues are emphasized in here.

Chapter 9: presents the main conclusions of this thesis work and future research directions.

The logical flow of the thesis chapters is summarized in Figure 1.1.

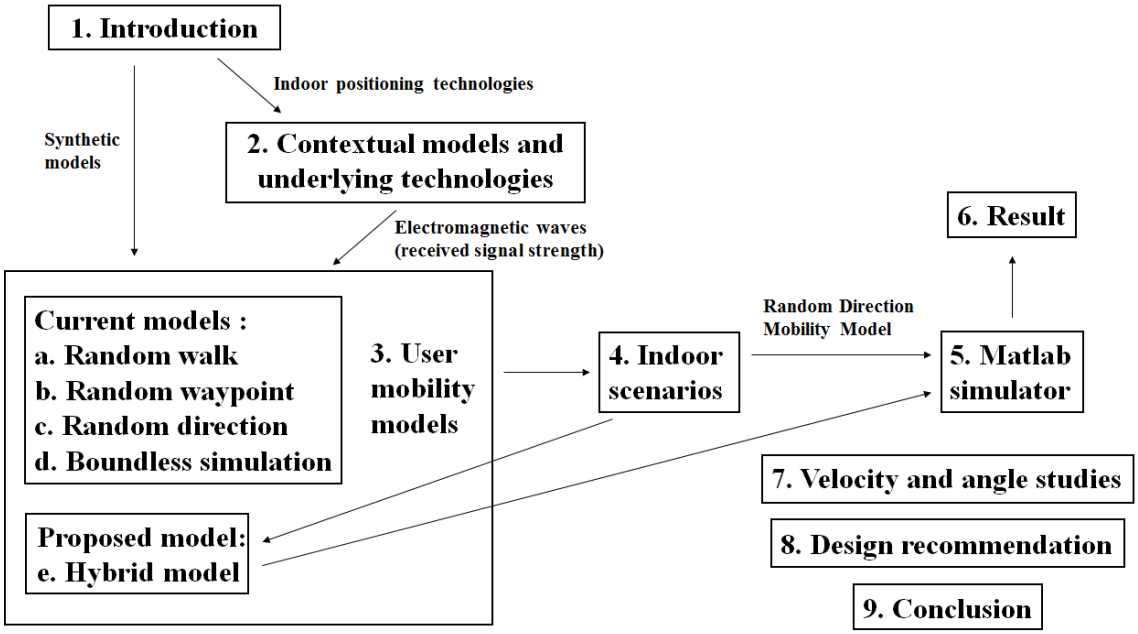

Figure 1.1: *The organization of the thesis.*

2. CONTEXTUAL MODELS AND UNDERLYING TECHNOLOGIES

Before further studying of human mobility models, investigation of available resources used in positioning technologies might help to understand better the indoor scenarios. This chapter reviews various technologies such as ultrasound, infrared ray, image or electromagnetic wave that are currently used in location services. In addition, extra comments are added to discuss the feasibility of utilization of these methods in real life.

2.1 Ultrasound

In nature, bats use ultrasounds as the means to execute echolocation actions. These actions help bats to navigate the forward path and to locate the position of prey in the night. Inspired by this, people developed similar navigation and position systems in the last hundred years. Here, an example (*Active Bat*) is shown to illustrate the principle and flexibility of ultrasound method under indoor positioning scenarios [1, 43].

Active Bat: The receivers of ultrasound on the ceiling form a grid; a user carrying wireless device broadcasts ultrasound signals cyclically; the distance between the user and receiver can be measured by the Time Of Arrival (TOA); as in many other systems the triangulation location algorithm is applied to compute the location of the user [18].

Comment: In essence, this technology calculates the distance by measuring the consumed time of transmitting signals, then the location is determined by applying the triangulation method. Specifically, the indoor coordinate initializes after the installation of several receivers on the ceiling. Next, the broadcasted ultrasound signals activate the receiver nodes, and through a series of algorithms this system selects three of the activated receivers and computes the user location. Moreover, the users can be tracked by storing positions of a users' movement track. Therefore, in this solution, the parameters such as the speed of ultrasound, the penetrability of

ultrasound, the interference level of background noise and the accuracy of receivers setup are crucial to the performance.

Ultrasound technology in localization has also been in used in *Cricket* [32, 33] and *Sonitor* [3].

2.2 Infrared radiation

Infrared radiation (IR) is an invisible radiation with longer wavelength than the visible light. Nowadays, the IR technology is used in a wide range of personal wireless platforms, which offer an alternative of achieving indoor positioning. This section presents the basis of IR-based indoor positioning technology via an instance of *Firefly* [22].

Firefly: Dozens of tags attached on the users' body emit in IR, and this radiation is captured by special cameras at fixed location. This system possesses the capability of tracking users' subtle motions. This motion tracker is usually used as an assistant of virtual reality related applications [18].

Comment: Generally, the IR-based technologies acquire users' location by observing tiny changes of the received IR. Due to the copyright and commercial reasons, this *Firefly* system has no detailed description. But from the above information, it is not hard to conclude that IR-based technology is restricted by conditions such as the intensity of background light, the angle of view, the penetrability of IR and the cost of the whole system.

IR technology in localization has also been used in *Active Badge* [19, 42].

2.3 Image

The human brain has the ability of determining movements by sensing difference between two images in the same scene. Similarly, by placing cameras and a central processor, this particular brain mechanism can be imitated for indoor positioning purpose. The following example introduces the fundamental of image-based indoor positioning technology.

Easy living: Two stereo cameras are set on the ceiling of a room, and these two are connected to a central processor. The action of a user coming into a room triggers the system and in the meantime the system marks this second as starting point. By

comparing the difference between two close frames, the system analyzes the current location of the user [18].

Comment: This technology relies basically on image processing and it has the advantage of not only locating the user, but also capturing the image of each user movement with a certain time precision. However, the disadvantage is quite obvious: processing considerable images requires substantial consumption of power and energy resource. Additionally the analysis of images might be affected by the light intensity.

Image-based technology in localization has also been explained and developed in [15, 25, 31].

2.4 Other electromagnetic waves

Unlike the indoor positioning solutions mentioned above, using electromagnetic waves as medium to achieve location services is a very popular way. Particularly, RFID, UWB and WLAN based indoor positioning technologies are one of the most active research areas. Given that this thesis mainly investigates the performance of human mobility models under WLAN situation, the discussion below focuses on the WLAN-based indoor positioning technology mainly.

RADAR: Three transmitters are set up at the beginning and the fingerprints grid is formed thereby. An user carrying a wireless device moves inside the coverage of transmitters signals. Considering that the strength of signals is inverse proportional to the distance between a transmitter and the user's device, the location of the user can be computed through the triangulation location method [18].

Comment: This might use a machine learning process. The fingerprints grid consists of received signal strength(RSS) at each point which is measured as the training sequence and the coordinates of each measured point. Afterward the positioning operation can be regarded as an estimation process.

3. USER MOBILITY MODELS

3.1 Overview

Before attempting to mimic human mobility patterns, we must find proof that human mobility has patterns to follow. In reference [17], the authors tracked 100,000 anonymous mobile phone users' location for six month. After modeling of numerous statistical data and appropriate scaling upon the model, they concluded that individual movement patterns have significant similarity. This conclusion, from the statistical point of view, gives a strong support to synthetic models.

This chapter is composed of two parts: a literature survey of human mobility models and a newly proposed human mobility model. In Section 3.2, we begin with the most widespread human mobility model namely the *Random Walk Mobility Model*. Later by adding one property to the *Random Walk Mobility Model*, we describe the second model, the *Random Waypoint Mobility Model*, in Section 3.3. In order to overcome weak points of the *Random Waypoint Mobility Model*, a third model called *Random Direction Mobility Model* is illustrated in Section 3.4. In Section 3.5, an ideal model namely the *Boundless Simulation Area Mobility Model* is given to describe the *Random Walk Mobility Model* from the mobile point of view. Last but not least, in Section 3.6 we present our proposed model, the *Hybrid Model* which is built to approach the real scenarios of human mobility inside buildings. Figure 3.1 shows the capacity of each model of describing various movements. Because the Boundless Simulation Area Mobility Model is an alternative interpretation of the Random Walk Mobility Model, the Boundless Simulation Area Mobility Model will not be shown separately in Figure 3.1. The Hybrid Model includes features originated from the Random Waypoint Mobility Model and the Random Direction Mobility Model, thus the circle of the Hybrid Model has overlaps with the above two models.

In Section 3.4 and 3.6, a hypothesis is posed for later study (i.e., different range velocities might have influence on the behavior of models under indoor scenarios). Besides, in these two sections, a Gaussian-like distribution is widely used for generating parameters such as velocities, moving time and pause time. In the Hybrid

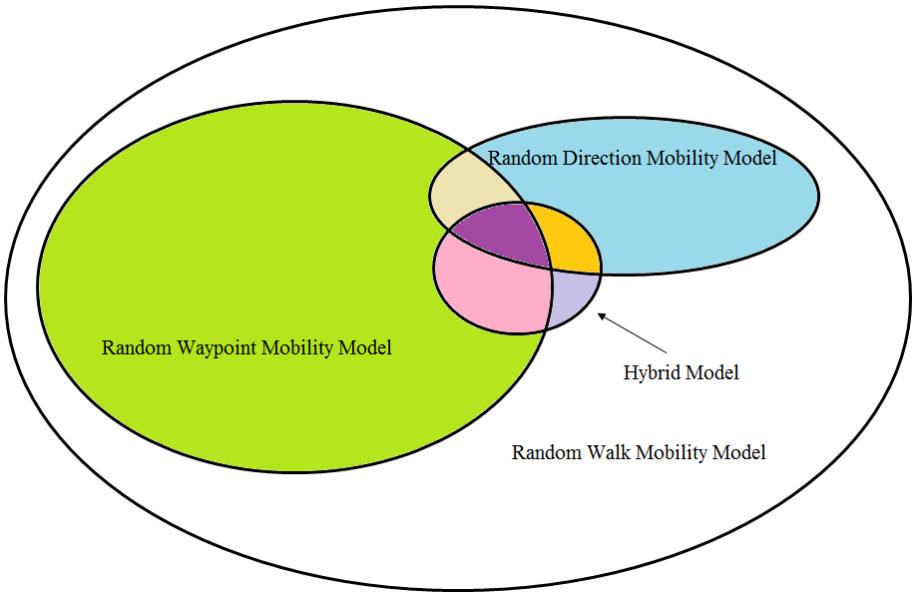

Figure 3.1: *Capacity of various movements.*

Model, a third dimension, namely the hight dimension, is introduced to mimic the scenario inside a building. It is to be noted that the above-mentioned notions, who will also appear in the rest of this chapter, will be explained in more detail in Chapter 4.

Notice: First, considering the fact that people have far greater displacement moving on the horizonal plane than the vertical plane, and that 2-D models have less computational complexity than 3-D models, the investigation of current models focuses on the 2-D models. In the proposal part, we discuss 3-D models, by tackling also some new angles in 3-D modeling that have not been discussed yet in the literature. Secondly, besides the above models, there are still other models, such as the Gauss-Markov Mobility Model, a model which contains knowledge of past location, velocities and angles [26]. However this thesis only discusses memoryless models and especially, the proposed Hybrid Model.

3.2 Random Walk Mobility Model

In 1905, when Einstein studied Brownian motion he revealed the relationship between the jump size and the time interval. That is, in other words, he mathematically described the Random Walk Mobility Model for the first time [13]. In this model, it is supposed that all the parameters are in the state of pure randomization. To be specific, a mobile starts from a random point with a random velocity, a random direction and a random moving duration. After one moving duration expires,

this mobile chooses another random velocity, another random direction and another random moving duration then it repeats the above process.

In practice, the Random Walk Mobility Model is often simulated in two implemented types: fixed duration and fixed displacement [12]. In the fixed duration case, we assume that each moving duration is constant, while the velocity and direction are random. In a mathematical way, this assumption can be expressed as follows:

$$\begin{cases} x_{n+1} = x_n + v_n cos\theta_n \Delta t \\ y_{n+1} = y_n + v_n sin\theta_n \Delta t \end{cases} \tag{3.1}$$

Correspondingly, in the fixed displacement case, it is assumed that each displacement for every resolution time interval is constant, while the direction is random, and that each step consists of a random number of above-mentioned time interval. Similarly, the mathematical expression is given by:

$$\begin{cases} x_{n+1} = x_n + \Delta d cos\theta_n k_n \\ y_{n+1} = y_n + \Delta d sin\theta_n k_n \end{cases} \tag{3.2}$$

In both eq. (3.1) and (3.2), (x_n, y_n) is the current position, (x_{n+1}, y_{n+1}) is the position of next state, θ is a random angle between heading direction of mobile and horizontal counterclockwise, v is a random scalar velocity, Δt is a constant duration for each step, Δd is a constant displacement for each time interval, k_n is equal to $\Delta t_n/\tau$ and Δt_n ia a random duration for each step, τ is a constant resolution time interval.

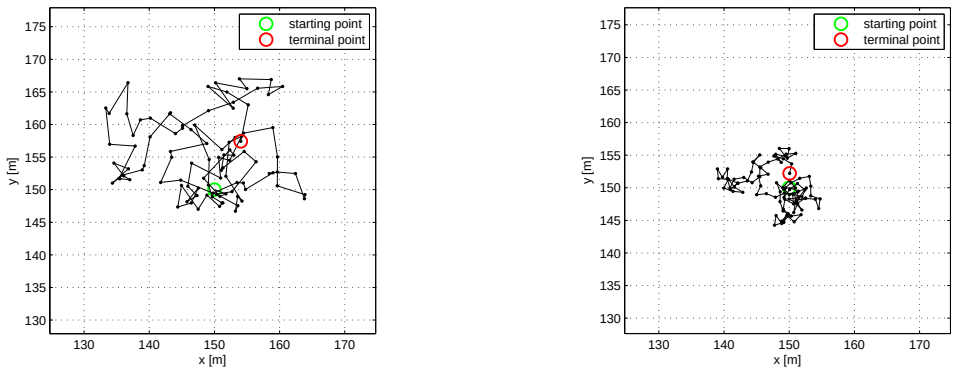

(a) Fixed duration for each step

(b) Fixed displacement for each step

Figure 3.2: *Simulation of one mobile track using 2-D Random Walk Mobility Model, the green circle represents the starting point and the red one represents the terminal point, each solid black point represents the sampled location data.*

In Figures 3.2(a) and 3.2(b), the initial position of the mobile is $(150, 150)$. In Figure 3.2(a), the total simulation time is 100 seconds, for each step the mobile has 1 second movement duration, velocities and angles are uniformly distributed in the interval $[0, 6](unit : m/s)$ and $[-\pi, \pi](unit : rad)$ respectively. Figure 3.2(b) gives a simplified example, the simulation has total 100 steps and for each step the duration only contains 1 time interval, in other words, k_n equal to 1. The fixed displacement for each resolution time interval is 1.5 meters, and the angles follows the same distribution as Figure 3.2(a).

Discussion: From the point of view of mimicking human movement patterns, the Random Walk Mobility Model shows redundancy description, such as sharp turns (i.e., big dynamic angle range within short time), fast-changing and large range of velocities and boundless area (i.e., neglect of obstacles in real life). As a common sense, human beings turn sharply with extremely low probability, and blocking objects, such as the sea and trees in the nature and buildings in the metropolis, are inevitable. In indoor scenarios, blocking objects are doors, walls and furniture. And Guinness records [5] of human running speed evidently prove the impossibility of random velocity for human beings. When reducing the duration for each step, a mobile modeled with a Random Walk Mobility Model (especially fixed displacement) will roam around the initial position. This characteristic fits the scenario of people in office hours (i.e., active in the small area) to some extent. Therefore, the Random Walk Mobility Model is ubiquitous, it contains the real human mobility patterns part whilst the redundancies part. All these considerations make this model too generic to fit restraints[1] of the indoor positioning.

3.3 Random Waypoint Mobility Model

This model is rather similar to the Random Walk Mobility Model, with the main differences that in the Random Waypoint Mobility Model there is a pause time parameter [23, 28, 29, 41].

Just like the Random Walk Mobility Model, when implementing a simulation of this model, we have to control certain random variables. Thus, there are two categories for implementation of the Random Waypoint Mobility Model as well: fixed duration and fixed displacement. In addition, if we simply plot a simulation of one mobile track using 2-D Random Waypoint Mobility Model on x-y plane, the mathematical expressions for this simulation are as the same as the section 3.2. Figures 3.3(a), 3.3(b) show one possible result of simulation for each condition:

[1] details about restraints of indoor scenarios will be narrated in Chapter 4.

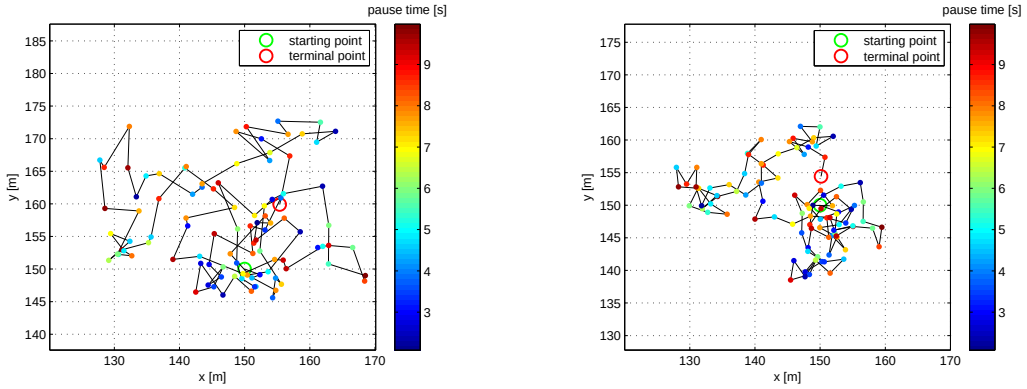

(a) Fixed duration for each step

(b) Fixed displacement for each step

Figure 3.3: *Simulation of one mobile track using 2-D Random Waypoint Mobility Model, the green circle represents the starting point and the red one represents the terminal point, different color of solid points represent the pause time.*

In Figures 3.3(a) and 3.3(b), the initial position of the mobile is $(150, 150)$. In Figure 3.3(a), the simulation includes 100 steps, for each step the mobile has 1 second movement duration, velocities and angles are uniformly distributed in the interval $[0, 8](unit : m/s)$ and $[-\pi, \pi](unit : rad)$ respectively. Figure 3.3(b) is still a simplified example and most of the parameters are the same as Figure 3.2(b) except that each displacement for a time interval is 3 meters.

Discussion: As said in the discussion part of section 3.2, the ability of a mobile roaming around a certain location for a long period indicates that this model is more suitable to model genuine human movement patterns than the Random Walk Mobility Model. Even though this model is a boundless model[2], the features such as the pause time are good to model the human mobility indoors. Therefore, we add this feature in the proposed model, Hybrid Model.

3.4 Random Direction Mobility Model

In the Random Walk Mobility Model and Random Waypoint Mobility Model, the mobile can move within a small area, a large area, or both, successively, depending on how the parameters are set. Due to this uncertainty, both these two models fail to simulate scenarios such as people mopping the floor, people touring in the exhibition etc. To overcome the high density of mobile location over partial area, the Random Direction Mobility Model was introduced in [35]. Since then, the Random Direction Mobility Model was also used in [14, 16, 36]. In this model, a mobile moves within a

[2]boundless models are not suitable for indoor positioning purpose, details will be presented in Chapter 4.

restricted area, it starts from a random point inside this area with random direction and random velocity, until it touches the boundary of the area it will not change velocity and direction.

In the practical simulation of this model, we increase the sampling frequency and limit the upper bound of the velocity in order to decrease the displacement for each step. There is a boundary ambiguity problem from the point of the view of the mobiles. This happens because in the implementation of this model we used a rectangle simulation area and a mobile moving within the rectangle area, the mobile has the possibility to move to the corner or the boundary. Imaging that the mobile is going to touch the corner or the boundary at a moment, then at the next moment, from the point of the view of the mobile, the mobile only knows that the position of itself is outside the rectangle area. Here the mobile does not know where it goes through the boundary. This happens because in the discretely collected data, the positions of a track of a mobile is actually not continuous. Hence the boundary ambiguity, in brief, is the issue of the unknown positions where the mobiles go through the boundary or corner.

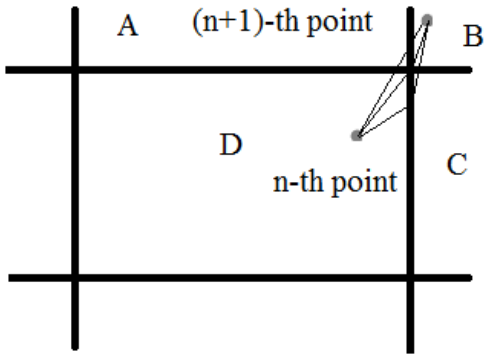

Figure 3.4: *Simulation area of Random Direction Mobility Model.*

In Figure 3.4, a mobile moves from the area D to the area B, there are several possibilities. For example, the mobile moves through the area C then ends into the area B, or the mobile moves to the corner and through the corner, ends into the area B, or the mobile passes through the area A then stops inside the area B. Due to the discrete positions data of a track, we only know the position of the n-th point and the position of the next point. The point of the intersection with the boundary is given by the estimation. In brief, the point of intersection is not absolute, which introduces uncertainty to the Random Direction Mobility Model.

As it was written in the Chapter 1, the movements of wireless devices carried by humans influence the WLAN environment. Here, in order to explore in what degree

the movements of devices influence the WLAN environment, we use the hypothesis that the different set of mobile speed ranges might have distinguishable impact on the behavior of measurements under wireless circumstance. Figure 3.5 illustrates one example by simply dividing models into large range velocity and small range velocity.

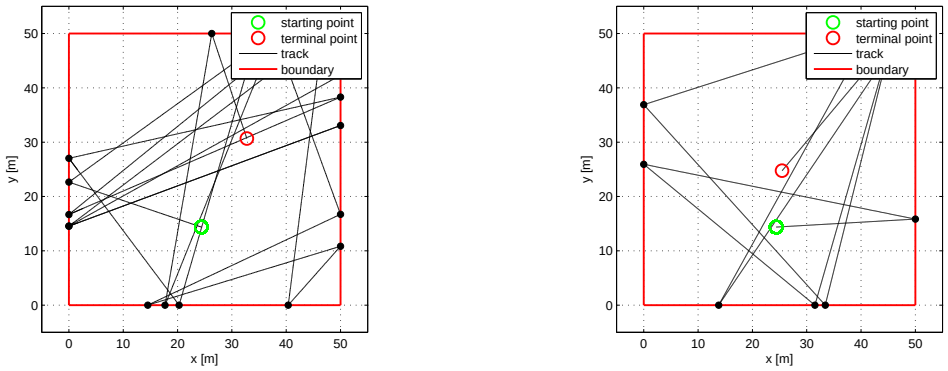

(a) Large velocity range ($0.5m/s$ *to* $3m/s$) (b) Small velocity range ($0.89m/s$ *to* $1.083m/s$)

Figure 3.5: *Simulation of one mobile track using 2-D Random Direction Mobility Model, the green circle represents the starting point and the red one represents the terminal point, each solid black point represents one touch of the boundary.*

In both Figures 3.5(a) and 3.5(b), the starting point is $(24.3716, 14.3716)$ $(unit : m)$, the simulation area is 50×50 $(unit : m)$, the angles follows a uniform distribution in the interval $[-\pi, \pi]$ $(unit : rad)$, the velocities are modeled according to a Gaussian-like[3] distribution shown in Figures 3.6(a) and 3.6(b), respectively for large velocity range and small velocity range. The small velocity range in this thesis is ($0.89m/s$ *to* $1.083m/s$) [7, 40]. We consider the elderly people case as the reference of the small velocity. By simply extending the range of elder speed, for example, ($0.5m/s$ *to* $3m/s$) is used as the comparison velocity range (i.e., the large velocity range).

Discussion: the Random Direction Mobility Model has boundaries, which makes it a good candidate for studying indoor scenarios with current indoor positioning techniques. Moreover, regarding the approximately even spread of mobile's positions, this model can be used to test to what extension a weak signal may impact on the WLAN-based indoor positioning technologies.

[3]Gaussian-like distribution will be detailed in Chapter 4.

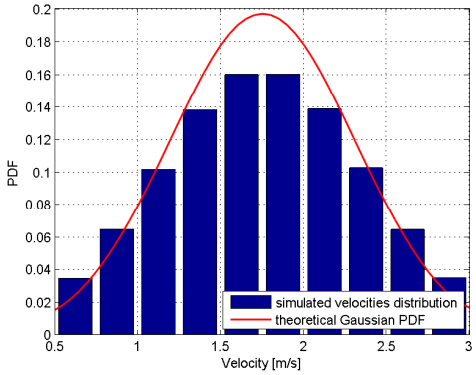

(a) Large Range Velocity Distribution: PDF of Gaussian-like Distribution for 2-D Random Direction Mobility Model

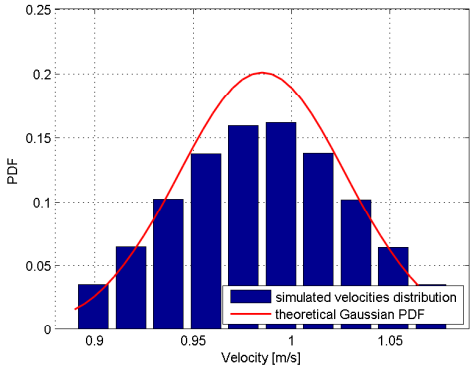

(b) Small Range Velocity Distribution: PDF of Gaussian-like Distribution for 2-D Random Direction Mobility Model

Figure 3.6: *The bar figure is the statistical performance of used velocities, the red line is the theoretical Gaussian distribution with the mean value and standard deviation of the velocity samples.*

3.5 Boundless Simulation Area Mobility Model

Imaging that we are mobiles, moving in the Boundless Simulation Area makes no difference from moving in the Random Walk Mobility Model. In this model, we use a rectangle area to form a doughnut-like 3-D object. In the Figure 3.7(a), by coinciding $\overline{AB}$ and $\overline{CD}$, and then coinciding $\overset{\frown}{AC}$ and $\overset{\frown}{BD}$, we get a doughnut-like area shown in Figure 3.7(b).

(a) a rectangle area

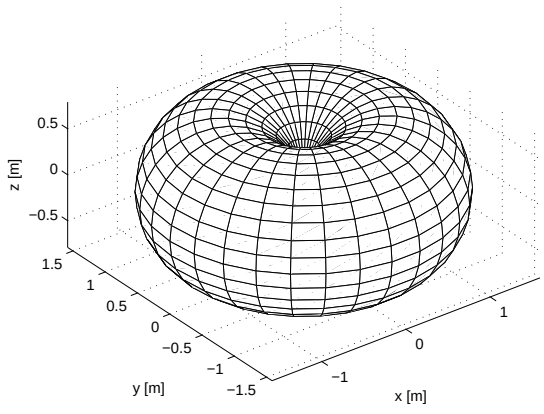

(b) a doughnut-like area

Figure 3.7: *The left plot shows a rectangle plane, and the right-hand plot shows a 3-D area formed from left figure.*

In this model, a mobile starts from a random position with random velocities, random directions and random moving duration. Once it touches the boundary, it

jumps immediately from current boundary to the opposite edge by using the third dimension. One example of simulation is shown in Figure 3.8:

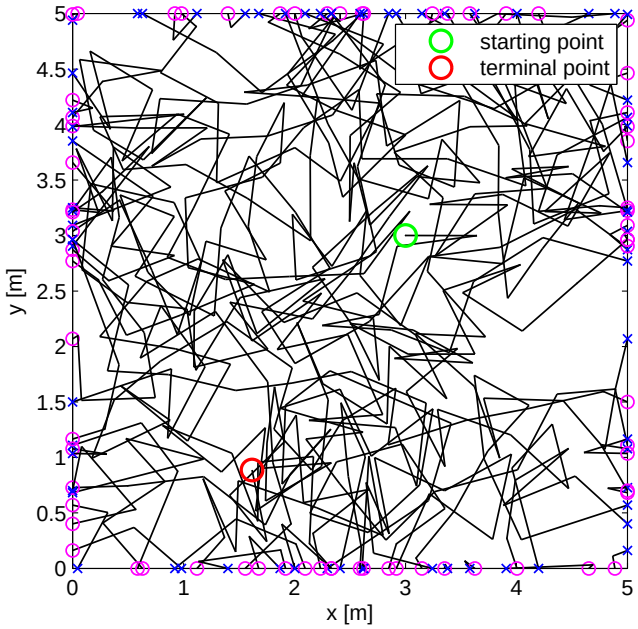

Figure 3.8: *Simulation of one mobile track using Boundless Simulation Area Mobility Model, the green circle represents the starting point and the red one represents the terminal point, the purple ◯ represents going out and the blue × represents going in.*

In Figure 3.8, the starting point is $(3, 3)$, the simulation area is $5 \times 5(unit : m)$, the number of total simulation steps is 500, the velocities and angles follow a uniform distribution in the interval $[0.5, 0.8](unit : m/s)$ and $[-2\pi, 2\pi](unit : rad)$ respectively.

Discussion: The Boundless Simulation Area Mobility Model is just a hypothesis that a mobile can use the higher dimension to continue its random walk. When applying this into indoor scenarios, it is obvious that human beings cannot jump instantly from one edge to the opposite edge. Therefore, this model is not suitable for simulating indoor scenarios.

3.6 Hybrid Model *(proposed)*

When we attempt to use a new synthetic model to describe human mobility patterns under indoor circumstance we assume, given that the existence of Random Direction Mobility Model, two restriction for indoor scenarios: firstly, this model should have a boundary in order to model obstacles (i.e., walls and doors in the building) in

daily lives, and secondly, the density of human historical plane positions should not be distributed completely even over the whole simulation area. This is based on the fact that out of the 24 hours in a day people are either in office hours or sleeping, and that an even density case is included in Random Direction Mobility Model. The Hybrid Model combines an analogous reaction mechanism from Random Direction Mobility Model when a mobile touches boundaries and a pause time which is a good feature of the Random Waypoint Mobility Model.

In detail, the pause time here is used to model the state of rest (e.g., after moving, people sit down for a while), and the reaction mechanism in the Hybrid Model is to simulate the time when people hit or approach obstacles. In section 3.4, we learned from the one possible expression of reaction mechanism, in the Random Direction Mobility Model, that a mobile does not change its state until it touches the boundary. Though this reaction already reflects the obstruction in real life, it is nevertheless rather improbable, because human will move away before hitting the object. So the nearest distance between the boundary and the mobile is added and defined by a random variable in the proposed model. The input and output variables of this model are defined by the Table 3.1.

Table 3.1: *the input and output variables of Hybrid Model*

Input	**Output**
simulation area	
number of floors	
height of each floor	
starting point	
velocity	(x_i, y_i, z_i)
angle	
moving time	
pause time	
minimum distance to the nearest boundary	

A mobile moves from a random starting point within the predefined simulation area, and it has a random velocity, an angle, a moving time, a pause time and a minimum distance to the nearest boundary. When the moving time expires it selects another velocity, angle and moving time, after this it holds still and waits the pause time to run out. While the mobile is moving, this model checks whether the distance between the mobile and the nearest boundary reaches a random predefined minimum distance or not. And if the situation is that the mobile reaches the nearest distance but the moving time or pause time is still on, this mobile will change its angle within a proper range and maintain the previous state except angles. Moreover,

this model is simply adding third dimension to mimic real indoor scenario, and this third dimension is generated by an algorithm that will be detailed in Chapter 4. One instance of simulation is illustrated in Figure 3.9.

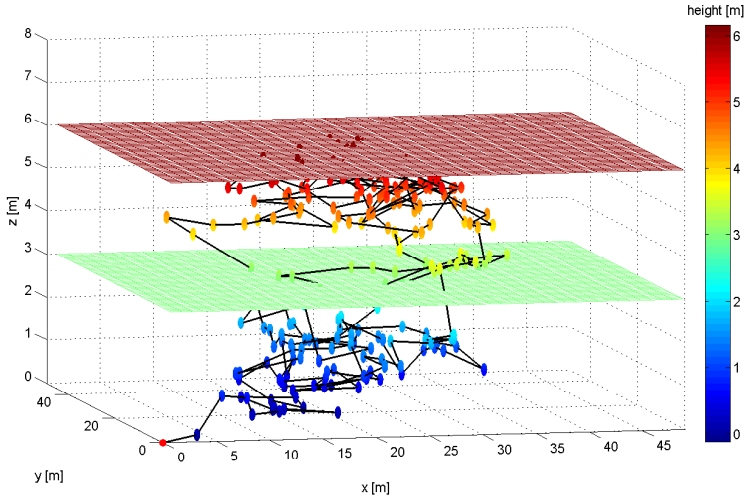

Figure 3.9: *Simulation of one mobile track using 3-D Hybrid Model (small velocity range), the red solid point represents the starting point and the color of each point represents height in this simulated building, the violet and green facets represent the simulated floors.*

In the simulation shown in Figure 3.9, the simulation area is $50 \times 50(unit : m)$, the starting point is $(0, 0, 0)$, the velocities basically follow the distribution showed in Figure 3.6(b), the angles follow a uniform distribution in the interval $[0, 2\pi](unit : rad)$, the moving time follows a Gaussian-like distribution in the interval $[3, 10](unit : second)$ showed in Figure 3.10(a), the pause time follows a Gaussian-like[4] distribution in the interval $[0.5, 30](unit : second)$ showed in Figure 3.10(b), the nearest distance follows the uniform distribution in the interval $[0.5, 20](unit : meter)$.

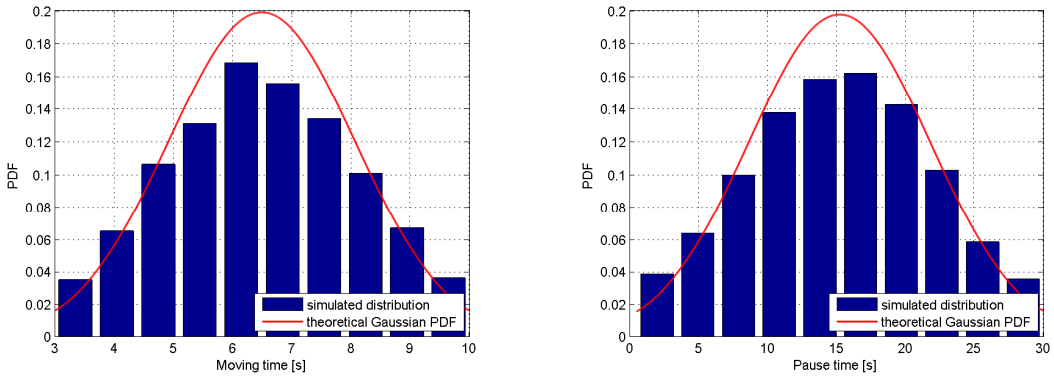

(a) PDF of the moving time (b) PDF of the pause time

Figure 3.10: *PDF of the moving time and pause time.*

Discussion: We mentioned in Section 3.4 that the Random Direction Mobility Model gives a mobile chances to cover every inch of simulation area with small time consuming. According to this characteristic, the Random Direction Mobility Model is used to describe scenarios such like tracks of cleaners inside a building. However, the Random Direction Mobility Model is not suitable to mimic the indoor office scenarios, which is a common case in the daily lives. Because in the office scenarios, a mobile is supposed to consume most of time inside a specific area. We can see from Figure 3.9, the Hybrid Model has the nonuniform distribution of positions of users. This feature fits the assumption of indoor office scenarios, which makes the Hybrid Model a candidate for the simulation of indoor office scenarios. In addition, the Hybrid Model has advantages suck like the minimum distance to the nearest boundary and the pause time, these advantages make the Hybrid Model become intelligent. But it cannot be denied that these advantages increase the complexity of the Hybrid Model.

3.7 Summary

This chapter starts by reviewing existing literature [12, 13, 14, 16, 28, 29, 35, 36, 41] followed by presenting the main ideas behind the Random Walk Mobility Model (Section 3.2), the Random Waypoint Mobility Model (Section 3.3), the Boundless Simulation Area Mobility Model (Section 3.5) and the Random Direction Mobility Model (Section 3.4). The presentation of the models is followed by demonstrating a feasible implementation method for each model. In Section 3.6, we propose a new model based on two assumptions and indoor scenarios characteristics.

The purpose of studying existed synthetic models and proposed models is to provide human mobility raw data for further simulation based research of indoor positioning methods. Hence the discussion about feasibility of current models in indoor scenarios is the main interest in this chapter. Table 3.2 lists the comparison among all the mobility models studied in this thesis.

[4] RWMM: Random Walk Mobility Model.
[5] RWPMM: Random Waypoint Mobility Model.
[6] RDMM: Random Direction Mobility Model.
[7] in the later simulation, the Random Direction Mobility Model is modified to be a 3-D model, details see Chapter 4 and Chapter 5.
[8] BSAMM: Boundless Simulation Area Mobility Model.
[9] HM: Hybrid Model.

Table 3.2: *Summary and comparison of models*

Models	Boundary	Pause Time	3-D Model	Suitable for Indoor Scenario	Specified Feature
RWMM[4]	No	No	No	No	Generic Model with large redundant description, because all parameters in this model are random it cannot be fully simulated.
RWPMM[5]	No	Yes	No	No	A pause time is introduced.
RDMM[6]	Yes	No	Yes[7]	Yes	A boundary concept is introduced and as well as a reaction mechanism after the user reached a boundary.
BSAMM[8]	No	No	No	No	An idealistic model concept, it simulates Random Walk within a limited area.
HM[9]	Yes	Yes	Yes	Yes	It comprehends most features from the other 5 models (above-mentioned) and it mimics the unevenly spread of human positions in indoor situation.

4. INDOOR SCENARIOS

4.1 Overview

In Chapter 3, we discussed current popular synthetic models and we proposed a new model. In this chapter we also present the complexity of indoor scenarios, the assumptions on human mobility patterns, and the path loss propagation models. This chapter includes the prerequisite knowledge for testing models by using the fingerprinting method in Chapter 5, and gives a thorough discussion of the matters in Chapter 3, such as the algorithm of generating the third dimension, the way of forming a Gaussian-like distribution and the indoor requirements.

4.2 Indoor environment

Indoor scenarios usually refer to the space inside a building. It is known that satellite based positioning systems are vulnerable inside buildings (Chapter 1), Here, we explain briefly how the indoor environment differs from the outdoor one.

In the indoor environment, the electromagnetic signals might be weakened in various ways. The indoor structure is more complex than the outdoor area. For example, there might be multiple cubicles in a common office, whereas outside area is normally open ground. Nowadays the indoor structure tends to be more and more complicated than ever. Multi-path interference is one of the main factors that severely degrade the performance of communications and locations. Buildings now are made of the concrete materials. The concrete has a strong ability to absorb electromagnetic energy. And as a simple rule, the higher frequency a signal has, the weaker penetrability it possesses. According to this principle and to the building materials, and given the fact that the radio frequency and microwave frequency are mainstreams of communications, it is obvious that electromagnetic signals suffers loss in indoor scenarios.

4.3 Assumptions about human mobility

After the brief introduction of indoor characteristics, this section mainly discusses the algorithms that are used to generate the height dimension and the Gaussian-like distribution. But first of all, some assumptions on selecting appropriate human mobility models are necessary. In this thesis, the most important property of a mobility model is to have a boundary. From Chapter 3, the only models which satisfy the boundary conditions are the Random Direction Mobility Model and the Hybrid Model. Other requirements of an indoor human mobility model differs from models to models. For example, the Hybrid Model is assumed to mimic the indoor office scenarios, thus it is supposed to fulfill the requirement that a mobile in the model has a nonuniform distribution of positions. Another example is the Random Direction Mobility Model, it is assumed that a mobile in the model has the trend to uniformly distribute the positions of a track.

4.3.1 The third dimension

In Chapter 5 simulation tracks from Random Direction Mobility Model and Hybrid Model have a third dimension. Here we will reveal the generator of this third dimension. In the height dimension generator, parameters such as the time of each step, the starting point of the third dimension and the minimum and maximum value of the third dimension are taken into consideration when we form the third dimension raw data.

In this generator, due to the lack of raw data from the real life, we simulate the third dimension increment by assuming it random and uniform. After the initial input variables are given, function *rand* creates a large number of candidate third dimension increments[10]. Then according to the condition if the third dimension value is larger than the maximum value (i.e., moving out the ceiling of building) or smaller than the minimum value (i.e., moving into the ground), the third dimension generator decides whether discarding this increment or not. Finally the output are the z values that satisfy the conditions. Figure 4.1 shows an example of third dimension value distribution.

[10]the number of this increments value should be large enough, so that after discarding some of values, we still have the same number of third dimension value as the number of other two dimension values. In this work we use 100 times of needed amount.

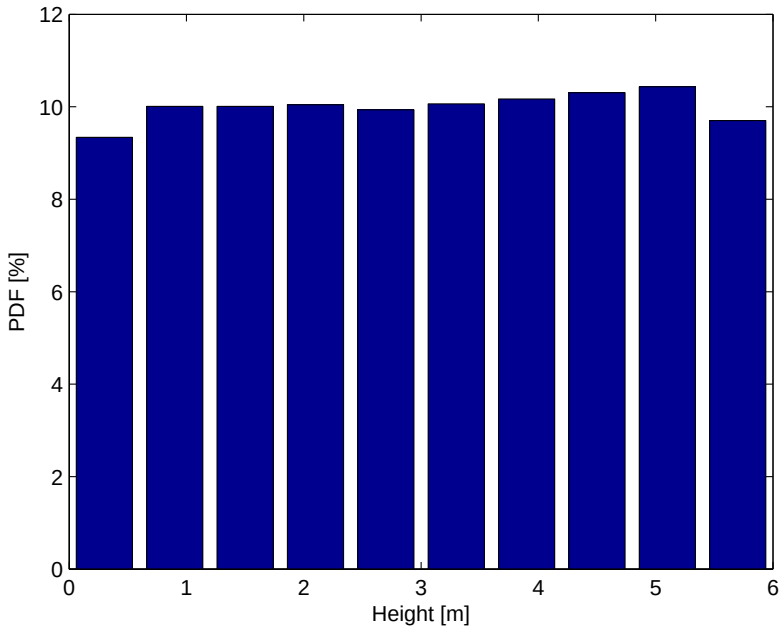

Figure 4.1: *The third dimension distribution: PDF of uniform distribution for the third dimension value, there are three floors and three meters for each floor in the simulation.*

4.3.2 Gaussian-like distribution

When using models to mimic human mobility patterns, not all of parameters should be distributed uniformly. In this thesis, the parameters such as the velocities, the moving time and the pause time follow Gaussian distribution. With 100% confidence level the confidence interval of Gaussian distribution function is $(-\infty, +\infty)$, however, this high confidence level is unnecessary in the practical simulation. The Gaussian-like distribution function is based on the standard normal distribution, it uses 95% confidence level[11] corresponding to confidence interval $[-1.96, 1.96]$. We assume the frequency of observing parameters is 95%, and in order to simplify the simulation, the values with 5% probability will not appear in the simulation.

In detail:

1. We use the function *randn* to generate 10 times of the numbers of needed variables. Because the function *randn* generates the standard normal distribution (i.e., the mean value equals to 0, the standard deviation equals to 1.), within

[11] As this design is for the simulation purpose, 95% confidence level is common [34, 10, 6] and high enough for this simulation, therefore in this function we use 95% confidence level and this parameter is able to be modified.

the interval $[-1.96, 1.96]$, the confidence level is 95%;

2. The generator abandons some variables by determining whether the generated variables are within the interval $[-1.96, 1.96]$;

3. The generator preserves the needed quantity of variables from step 2;

4. By comparing $[-1.96, 1.96]$ with the target interval, the generator adjusts the samples inside $[-1.96, 1.96]$ in order to fit the target interval, the target interval here refers to the desired sample space interval.

With an example, the process of generating Gaussian-like distribution is illustrated. Assuming we have a sample space (e.g., $[-2, 2]$), we want to pick samples from the space (i.e., $[-2, 2]$) and the picked samples should be Gaussian-like distributed. In the Gaussian-like generator we used, first we form 10 times of the numbers of the needed variables by using the function *randn*, secondly we abandon some variables that are not within the interval $[-1.96, 1.96]$, thirdly we pick needed numbers of variables after the second step (e.g., one variable is 1.5), fourthly we scale the picked variables. In the fourth step, we calculate the mean value between the upper bound and lower bound of sample space, in this case, the mean value is $(-2 + 2)/2 = 0$, then we use $(2 - ((-2 + 2)/2))/1.96 = 1.0204$ as scale factor to multiple the picked variables in the third step (i.e., $1.5 \times ((2 - ((-2 + 2)/2))/1.96) = 1.5306$), finally we plus the mean value and the result of multiplication (i.e., 1.5306+0=1.5306). Figure 3.6(a), Figure 3.6(b), Figure 3.10(a) and Figure 3.10(b) are generated by the above algorithm.

4.4 Path loss models

In Chapter 5, we will use indoor fingerprinting method to test the performance of selected human mobility models. Hereby this section presents the corresponding fundamental knowledge of path loss model as well as a modified version applied in indoor scenarios. The traditional path loss model is related with two modeling parts [38]: $P_{T_{ap}}$, namely the ap-th AP transmitted power, and n_{ap}, namely the path loss coefficient of the ap-th AP.

The RSS in each measurement point is directly related to the Euclidian distance $\sqrt{(x_i - x_{ap})^2 + (y_i - y_{ap})^2 + (z_i - z_{ap})^2}$, where the (x_i, y_i, z_i) is the position of the i-th measurement point (i.e., position of the i-th fingerprint) and (x_{ap}, y_{ap}, z_{ap}) is the position of the ap-th AP. The $P_{T_{ap}}$ varies from AP to AP within a certain range,

and the n_{ap} is simply assumed to be different from AP to AP as well. Then we form the eq.(4.1) for fingerprints RSS $P_{i,ap}$:

$$P_{i,ap} = P_{T_{ap}} - 10n_{ap}\log_{10}\sqrt{(x_i - x_{ap})^2 + (y_i - y_{ap})^2 + (z_i - z_{ap})^2} + \eta_{i,ap} + \xi_{i,ap} \quad (4.1)$$

In this equation, $\eta_{i,ap}$ is a noise term modeling the shadowing and fading. It is Gaussian distribution of zero mean and σ_{ap} standard deviation (unit: dB). To be clarified, without abundant database of modeling $\eta_{i,ap}$, we simply assume the variance σ^2 is constant. $\xi_{i,ap}$ is to characterize the floor loss parameter, because in a relative open and multi-floors building ceilings between floors are the main barriers against the transmission of signals.

Correspondingly, we can derive received signal strength (RSS) at the (x, y, z) position, (x, y, z) is the position of a mobile in a track. The equation of RSS R_{ap} is illustrated as below:

$$R_{ap} = P_{T_{ap}} - 10n_{ap}\log_{10}\sqrt{(x - x_{ap})^2 + (y - y_{ap})^2 + (z - z_{ap})^2} + \eta_{ap} + \xi_{ap} \quad (4.2)$$

The eqs.(4.1) and (4.2) will be used in Chapter 5 to form the fingerprints training sequence and to compute the RSS of one mobile in a track[12].

4.5 Indoor fingerprinting

A fingerprinting algorithm is usually used in the indoor positioning technologies under WLAN environment. It requires that a random location in this indoor area can hear at least one AP. The process of fingerprinting has two phases:

- **A training phase**: This is used to form a grid of prior RSS measurements from all APs in a certain building or region;
- **An estimation phase**: This focuses on comparing the RSS of a mobile with training database formed in the training phase; this comparison will provide an estimate for the mobile location.

[12] details see Chapter 5

We remark that the fingerprint grid is virtual, people cannot actually touch the grid or see the grid in the air.

4.5.1 Training phase

The purpose of the training phase is to generate a database (i.e., matrix $(\mathbf{X_i}, \mathbf{Y_i}, \mathbf{Z_i}, \mathbf{P_{i,ap}})$) containing the prior RSS measurement and the position information. In this phase, we assume the location of APs is fixed.

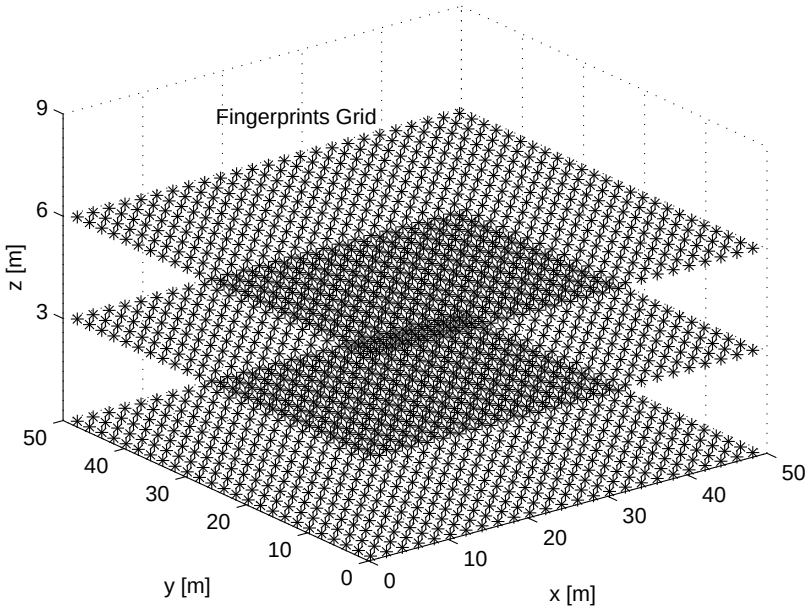

Figure 4.2: *One possible way to set up fingerprint grid, one $*$ represents a measurement point in the grid.*

The training sequence is de facto a reference data, it includes both the position information and RSS information matrix heard from APs. In the fingerprint algorithm, the location of APs is irrelevant to the whole positioning process but it matters when some corners of this indoor area cannot hear AP. One of possible fingerprinting grid [13] is shown in Figure 4.2.

4.5.2 Estimation stage

After the training database is formed, the indoor fingerprint positioning environment is ready. When a mobile moves into this area, the receiver attached on the mobile

[13] it is only possible in theory, in practice it is almost impossible to collect such nicely uniformly-spaced fingerprints, some of them will be missing, unless the uniform spacing between points is very large.

downloads the prepared database which was generated in the training phase, then it compares the received RSS vector information with the database. The comparison can be done for example via Euclidian distances, rank-based or via Gaussian likelihoods. The comparison gives all the candidate positions. Eventually according to a predefined rule, the receiver sorts this potentials and calculates the final prediction position of this mobile at that moment.

Firstly a mobile in this fingerprint scenario records all heard RSS value automatically and it stores them as a vector which includes the *ap*-th AP and corresponded RSS value (i.e., $[ap; \mathbf{R_{ap}}]$ in the eq.(4.2)). Secondly, the system applies the Gaussian likelihood function to estimate the probability of position in the grid. In this step, the system usually gives more than one candidate position to achieve high accuracy. Thirdly, by a certain rule the system calculate the position, for example, it calculates the arithmetic average of the first four high probably candidates as the predicted position.

The Gaussian likelihood function L_i in i-th point is shown below, the σ_{ap}^2 is the shadowing variance:

$$L_i = \sum_{heard\ ap} \log_{10} \left(\frac{1}{\sqrt{2\pi\sigma_{ap}^2}} e^{-\frac{\left(R_{ap}-P_{i,ap}\right)^2}{2\sigma_{ap}^2}} \right) \tag{4.3}$$

Here we give an example how to apply this equation. Let us assume two fingerprint points, a: [1,3,7; -30,-70,-56] and b: [1,5,7; -45,-20,-68], and one track point, m: [3,7; -60,-70]. The first step is to find the same heard AP for both the fingerprint and the mobile. In a and m it is 3rd and 7th AP but in b and m it is 7th AP only. Then by assuming the involved noise is 10 dB and constant, we can get $L_a = -3.07 - 5.16 = -8.23$ for a and m, $L_b = -0.99$ for b and m. Afterwards, by maximizing the L_i ($i = a$ *or* $i = b$) we obtain the best candidate in this algorithm, that is b in this case. This algorithm reveals that even though a mobile shares more heard APs with some fingerprints than others, these fingerprints might not be the most optimized solution.

4.6 Summary

At the beginning of this chapter, the indoor was introduced to give an general perception that indoor scenarios are complex and not applicable for satellite based positioning system. Then we described and explained how the third dimension and Gaussian-like distribution are generated. It should be mentioned that the 95%

confidence level is just an assumption in this thesis work and it is not the focal point, when there are no more other confidence level provided for comparison. After that, the prerequisite knowledge for the later chapter, the classical path loss with floor loss model was presented. In the last part, the notion of indoor fingerprinting was given in detail.

Eqs. (4.1), (4.2) and (4.3) are the most important ones in this chapter and will be used in Chapter 5 and 6.

5. BUILT MATLAB SIMULATOR

5.1 Overview

This chapter presents the Matlab simulator built within this thesis work, which includes mobility modeling and fingerprinting. In Chapter 3, we demonstrated the results of the implementation through our simulator. Here we focus on how the simulator is built and furthermore we discuss the simulator of the fingerprinting. Figure 5.1 shows the used simulators in this thesis work and their relationship correspondingly.

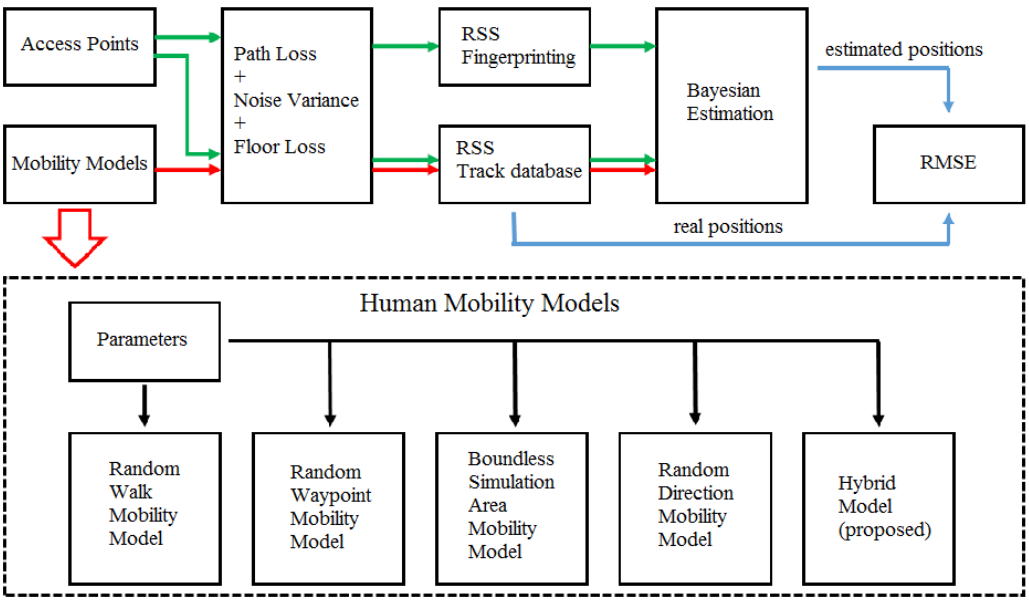

Figure 5.1: *The organization of simulators.*

5.2 Access Points setup

In this simulation, it is assumed $l_1 \times l_2$ $(unit : m)$ simulation area, N floors in a building and l_3 meters for each floor, C m^2 coverage per AP on the horizontal plane

and $[P_1, P_2]$ $(unit : dB)$ power range. Specifically, the positions of APs are uniformly distributed random variables and the power levels of APs are uniformly distributed random variables within the above range as well. There are two main reasons why the uniform distribution rather than the Gaussian distribution is selected. First the uniform distribution is less computation complex than the Gaussian distribution when they applied in the simulator. Secondly using the uniform distribution the APs can cover the whole area with smaller number of APs than using the Gaussian distribution. One example of these parameters is shown in Table

Table 5.1: *One example of Access Points parameters*

Parameters	**Values**
l_1 (m)	50
l_2 (m)	50
N	3
l_3 (m)	3
C (m^2)	400
$[P_1, P_2]$ (dB)	[-45,-30]

When deploying APs, the rule of thumb is that using relative few APs to cover the simulation area. From 2-D view the building can be considered as a rectangle area. Figure 5.2 shows the overlap of the coverage areas of APs on 2-D area, the rectangle is the simulation area, the circles are the coverage areas of APs. The grass green area represents the simulation area, the grey areas represent the overlap areas inside the simulation area, the brown areas represent the overlap areas outside the simulation area and the coverage areas APs outside the simulation area. With Figure 5.2, we can simply explain the rule of deploying APs, that the fewer the grey and brown areas are, the better the deployment is. However, it is not possible to eliminate the grey areas completely because of the spherical radiation shape of electromagnetic waves. In 3-D view, the coverage of APs supposes to be spherical shape, thus we calculate the availability of APs in eq. (5.1) using the volume of APs radiation.

Figure 5.3 shows the used deployment in this thesis work. If we assume Figure 5.2 in 3-D, the volume of the cubic simulation area is V_{cube}. The sum of each AP coverage is V_{sum}, the substraction between V_{sum} and V_{cube} might, to some extent, evaluate the degree of overlap namely coverage margin $M_{coverage}$. In eq. (5.1), r_{ap} is the effective radiation radius of the ap-th AP, $(x_{max}, y_{max}, z_{max})$ is the maximum value of simulation space in three dimension respectively.

$$M_{coverage} = \sum_{ap=1}^{n} \frac{4}{3}\pi r_{ap}^3 - x_{max}y_{max}z_{max} \tag{5.1}$$

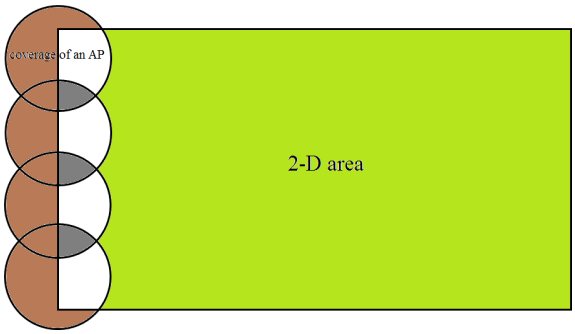

Figure 5.2: *Principle of APs deployment, the rectangle area is the simulation area, the circles are the coverage area of APs, the grey areas are overlapped coverage areas.*

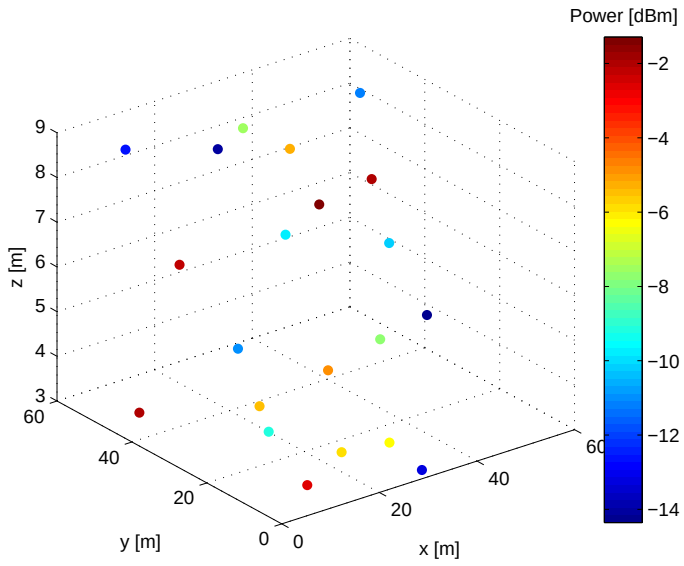

Figure 5.3: *APs deployment used in this thesis work, the solid color points represent APs and APs transmitted power are seen in the right-hand side color bar.*

In Table 5.2, we show a comparison between two groups: 3 scenarios of simulated data and 2 scenarios with real-field data. For each group, we illustrate the ratio between $M_{coverage}$ and V_{cube}, ratio between mean number and total number of heard APs per fingerprint, ratio between median number and total number of heard APs per fingerprint, standard deviation of AP number per fingerprint. The ratio between $M_{coverage}$ and V_{cube} intuitively indicates that to what extent the coverage areas of APs are utilized. The statistics of number of heard APs per fingerprint shows shows how the number of heard APs per fingerprint varies under a certain deployment or density of APs. The statistics gives the reference to the preliminary judgement that whether the deployment is good or not. Usually the larger the mean (or median) number of heard APs per fingerprint is, the better the deployment is. But when we consider the cost of the deployment, the mean (or median) number of heard APs

per fingerprint should not be too large. This happens because the mean number or median number is proportional to the density of APs.

Table 5.2: *Comparison for 3 scenarios of simulated data and 2 scenarios with real-field data*

Parameter	**Simulated scenarios**			**Real-field data**	
	2 *dB*	10 *dB*	40 *dB*	building 1	building 2
$M_{coverage}/V_{cube}$ [ratio]	4.6168	4.6168	4.6168	×	×
Mean number/total number [14] [ratio]	0.7712	0.8369	0.6911	0.1350	0.1352
Median number/total number [14] [ratio]	0.7619	0.8571	0.7143	0.1303	0.1243
standard deviation of heard APs number per fingerprint [14]	1.7169	1.6173	2.0255	10.8383	19.0334

**Important*: Once the deployment of APs is finished, all the following simulation should use exactly the same deployment and same power level.

In Table 5.2, 2 dB, 10 dB and 40 dB noise variance are chosen to show the low noise level, medium noise level and high noise level scenarios respectively. Two real databases [38, 39] are collected from Tietotalo building (i.e., building 1) and Sahkotalo building (i.e., building 2) in Tampere University of Technology. Under the fingerprint algorithm and the Bayesian estimation, in building 1 the positioning accuracy is around 5 meters and in building 2 the accuracy is approximate 10 meters. We remark that, due to the irregular shape of building 1 and building 2, the ratio of $M_{coverage}/V_{min}$ cannot be given.

From the columns of 'Real-field data' in Table 5.2, we can tell that, the values of 'mean number/total number' and 'median number/total number' are almost the same for both building 1 and building 2. However the 'standard deviation of heard APs number per fingerprint' varies significantly from building 1 to building 2, and specifically the higher accuracy positioning (i.e., building 1 with around 5 meters accuracy) comes with lower 'standard deviation of heard APs number per fingerprint' based on these two real database. In addition, as it was mentioned before, the building 1 with 0.1350 'mean number/total number' ratio and 0.1303 'median number/total number' ratio achieved 5 meters accuracy under the Bayesian estiamtion,

[14] All these three statistics refer to the number of heard APs per fingerprint point. 'mean number/total number' is a ratio between the mean value and the total number of heard APs per fingerprint point, 'median number/total number' is a ratio between the median value and the total number of heard APs per fingerprint point, 'standard deviation of heard APs number per fingerprint' is the standard deviation of number of heard APs per fingerprint point.

therefore when these two values of simulation or real deployment are higher than the corresponding values of the building 1, they are feasible.

In the simulation scenarios, the 'mean number/total number' ratio and 'median number/total number' ratio of all noise circumstances are considerably higher than those in building 1, and the 'standard deviation of heard APs number per fingerprint' of all are far smaller than the standard deviation in building 1. Therefore, under the simulated APs deployment, the high positioning accuracy (i.e., 5 meters accuracy or a better accuracy) is able to achieve.

Figures 5.3, 5.4, 5.5, 5.6, 5.7 give some statistical information about the relationship between the AP density in a building and achievable positioning accuracy from fingerprints' point of view. Among them, Figures 5.3, 5.4, 5.5 present the analysis of simulated APs deployment, Figures 5.6, 5.7 show the analysis of real APs deployment. To be specific, in all these 5 group figures the sub-figure *a* says how many percentage of total APs an arbitrary fingerprint point can hear. One fingerprint point can hear more than one, because for each one fingerprint point, it usually can hear more than one power level, the sub-figures *b,c,d* give the statistical description of the mean power level, the median power level and the standard deviation of heard APs power level per fingerprint respectively. We remark that, in the first three group simulation figures, it is assumed the sensitivity of receivers is -100 dBm.

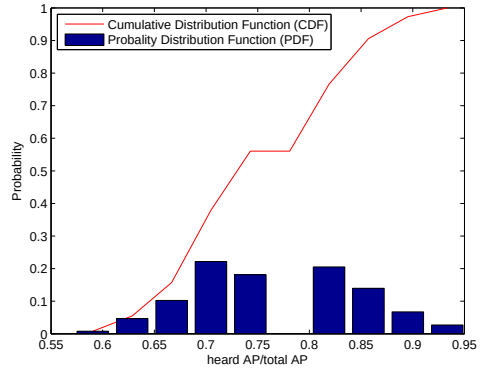

(a) Ratio between number of heard APs and total APs per fingerprint point

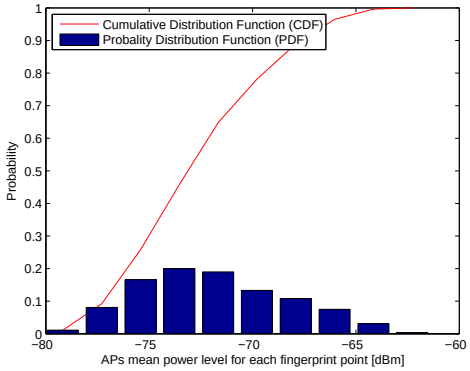

(b) Mean heard power level per fingerprint point

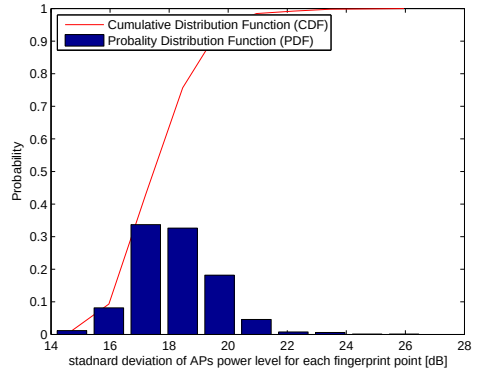

(c) Standard deviation of heard power level per fingerprint point

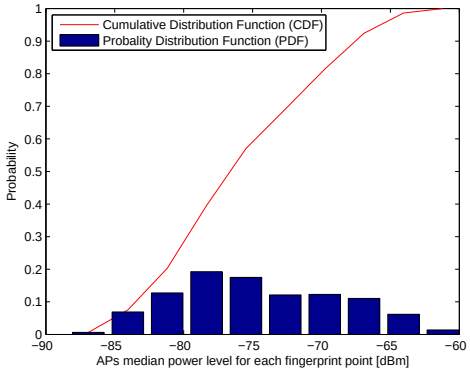

(d) Median heard power level per fingerprint point

Figure 5.4: *2 dB noise level (receivers sensitivity: -100 dBm).*
This case is used to simulate scenarios with low noise power level. It can be simply thought as 'noise free' situation so that we can consider this one as a reference for further comparison. In Figure 5.4(a), most fingerprint points can hear 70% - 85% *of total APs, in Figure 5.4(b), most fingerprint points can hear* $-75dBm$ - $-70dBm$ *mean power level (the transmitted power level is* $-15dBm$ - $0dBm$*), in Figure 5.4(c), the standard deviation of power level from various APs per fingerprint point is around 18 dB, in Figure 5.4(d), most fingerprint points can hear* $-80dBm$ - $-75dBm$ *median power level.*

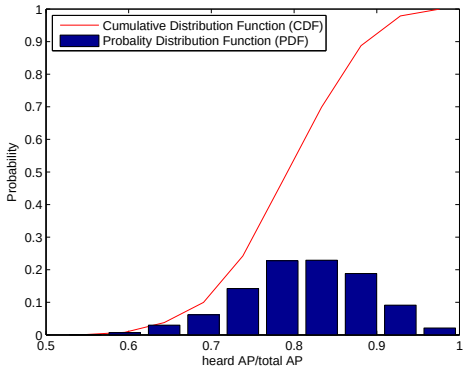

(a) Ratio between number of heard APs and total APs per fingerprint point

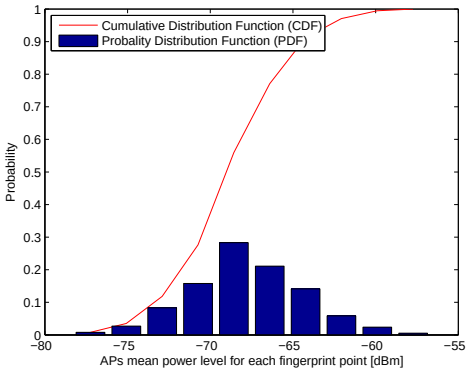

(b) Mean heard power level per fingerprint point

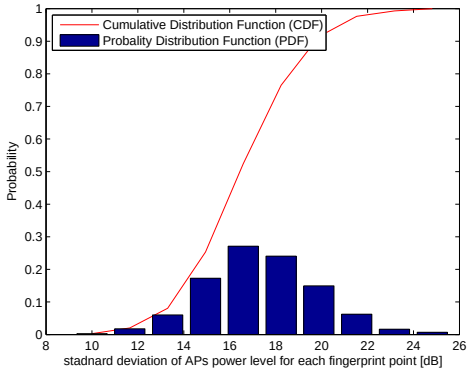

(c) standard deviation of heard power level per fingerprint point

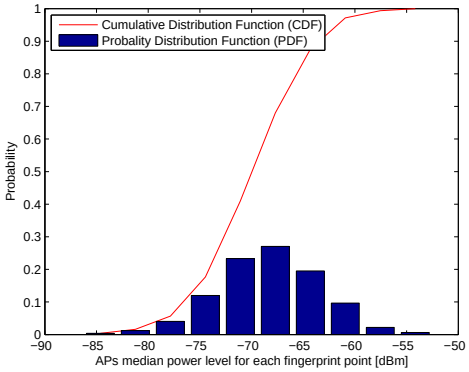

(d) Median heard power level per fingerprint point

Figure 5.5: *10 dB noise level (receivers sensitivity: -100 dBm).*
This case is used to simulate scenarios with medium noise power level. It can be simply thought as 'noisy' situation in the simulation. In Figure 5.5(a), most fingerprint points can hear 80% - 90% *of total APs, in Figure 5.5(b), most fingerprint points can hear* $-70dBm$ - $-65dBm$ *mean power level (the transmitted power level is* $-15dBm$ - $0dBm$*), in Figure 5.5(c), the standard deviation of power level from various APs per fingerprint point is around 17 dB, in Figure 5.5(d), most fingerprint points can hear* $-70dBm$ - $-65dBm$ *median power level. Compared with 2 dB noise level case, this 10 dB one indicates that the statistics of heard AP power level are proportional to the noise level. Another proof of this conclusion will be presented in the next group of figures.*

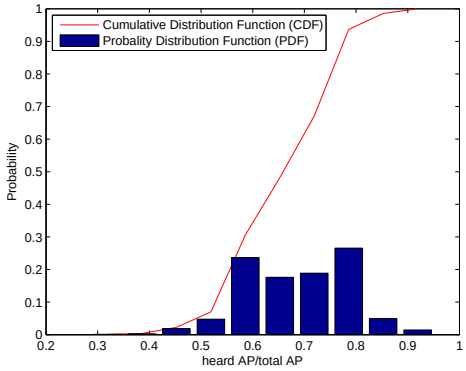

(a) Ratio between number of heard APs and total APs per fingerprint point

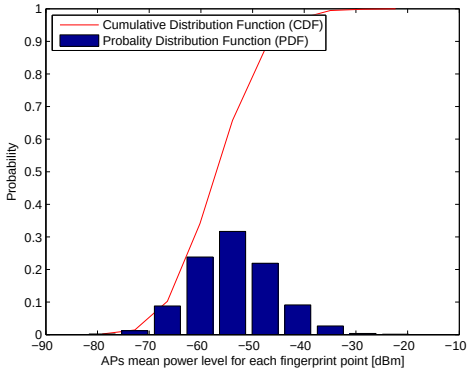

(b) Mean heard power level per fingerprint point

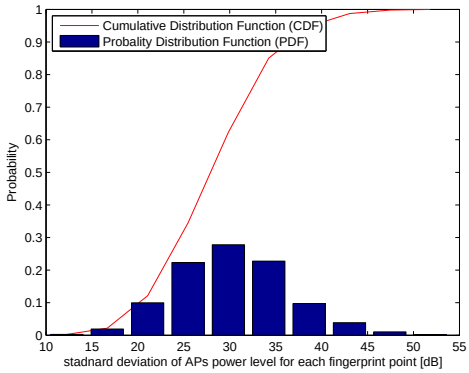

(c) standard deviation of heard power level per fingerprint point

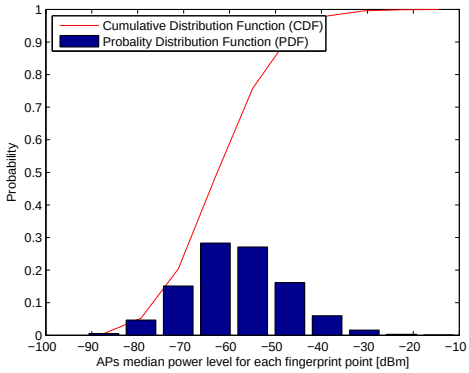

(d) Median heard power level per fingerprint point

Figure 5.6: *40 dB noise level (receivers sensitivity: -100 dBm).*
This case is used to simulate scenarios with high noise power level. It can be simply thought as 'extremely noisy' situation in the simulation. In Figure 5.6(a), most fingerprint points can hear 60% - 80% *of total APs, in Figure 5.6(b), most fingerprint points can hear* $-60dBm$ - $-50dBm$ *mean power level (the transmitted power level is* $-15dBm$ - $0dBm$*), in Figure 5.6(c), the standard deviation of power level from various APs per fingerprint point is around 30 dB, in Figure 5.6(d), most fingerprint points can hear* $-70dBm$ - $-50dBm$ *median power level. Through simply comparison with the 2 dB and 10 dB figures, it is not difficult to assess that the standard deviation is proportional to the noise level; moreover with the increase of the noise level, the number of heard APs, mean and median value of power level per fingerprint point tends to be larger.*

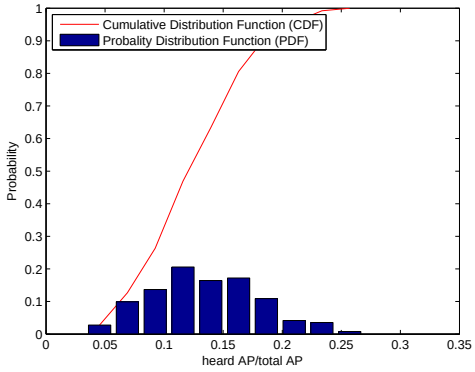

(a) Ratio between number of heard APs and total APs per fingerprint point

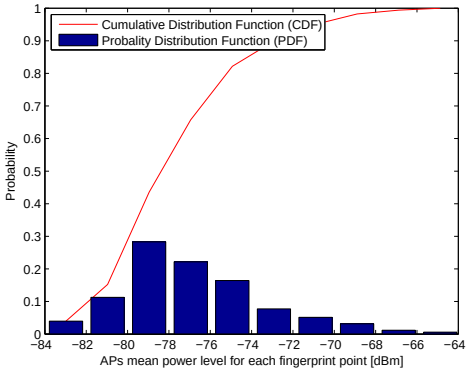

(b) Mean heard power level per fingerprint point

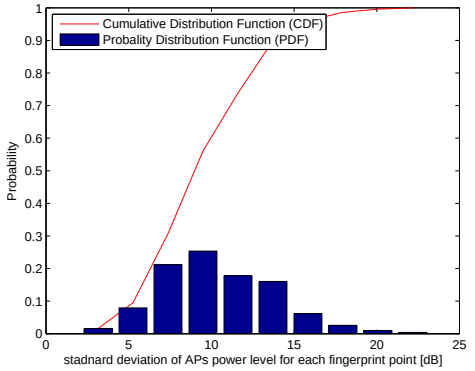

(c) standard deviation of heard power level per fingerprint point

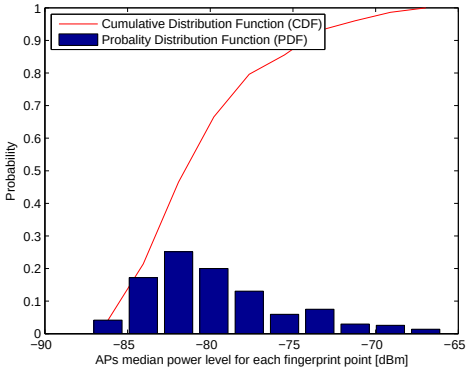

(d) Median heard power level per fingerprint point

Figure 5.7: *Building 1 with unknown noise level (receivers sensitivity: -100 dBm). This case is a statistical modeling of real data collected from building 1. It has better positioning accuracy under Bayesian estimation method than building 2. In Figure 5.7(a), most fingerprint points can hear* 10% - 20% *of total APs, in Figure 5.7(b), most fingerprint points can hear* $-80dBm$ - $-76dBm$ *mean power level (the transmitted power level is unknown, and is estimated with range* $-15dBm$ - $0dBm$*), in Figure 5.7(c), the standard deviation of power level from various APs per fingerprint point is around 9 dB, in Figure 5.7(d), most fingerprint points can hear* $-85dBm$ - $-80dBm$ *median power level.*

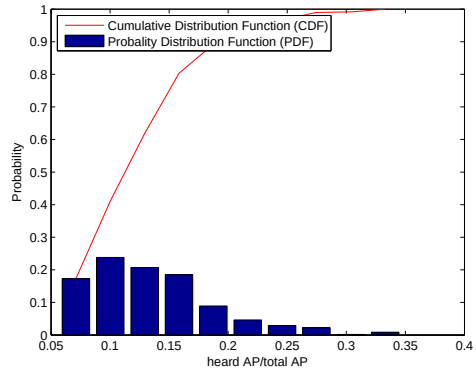

(a) Ratio between number of heard APs and total APs per fingerprint point

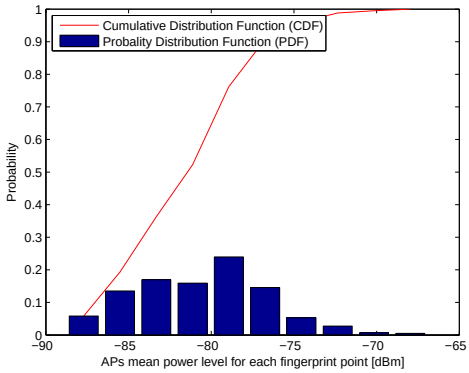

(b) Mean heard power level per fingerprint point

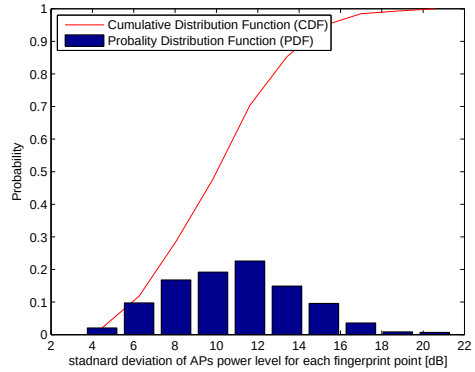

(c) standard deviation of heard power level per fingerprint point

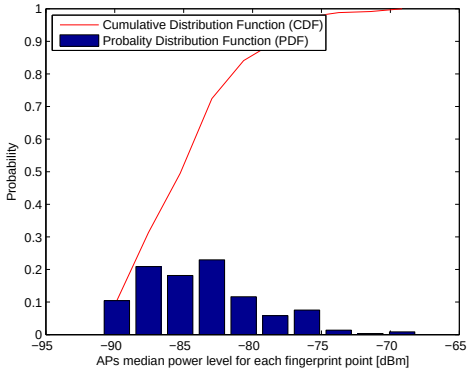

(d) Median heard power level per fingerprint point

Figure 5.8: *building 2 with unknown noise level (receivers sensitivity: -100 dBm). This case is a statistical modeling of real data collected from building 2. In Figure 5.8(a), most fingerprint points can hear* 5% - 15% *of total APs, in Figure 5.8(b), most fingerprint points can hear* $-85dBm$ - $-75dBm$ *mean power level (the transmitted power level is unknown, and is estimated with range* $-15dBm$ - $0dBm$*), in Figure 5.8(c), the standard deviation of power level from various APs per fingerprint point is around 12 dB, in Figure 5.8(d), most fingerprint points can hear* $-90dBm$ - $-80dBm$ *median power level.*

Analysis of Figures 5.3, 5.4, 5.5 reveals that number of heard APs increases when the noise power level changes from 2 dB to 10 dB and 40 dB, the mean value, median value and standard deviation of heard power level per fingerprint point grow along with the increase of noise power level as well. In Figures 5.6 and 5.7, the most frequent ratio between the heard APs and total APs (i.e., 0.1-0.15 ratio) is smaller than the most frequent ratio between the heard APs and total APs in Figures 5.3, 5.4 and 5.5 (i.e., 0.6-0.9 ratio). The standard deviation of the heard power level per fingerprint point in building 1 is smaller than in building 2. The mean value and median heard power level per fingerprint point in building 1 are stronger than in building 2. Figures 5.6 and 5.7 describes the characteristics of data collected in real life scenario, the following analysis of simulated APs deployment is based on them.

Intuitively, from the user point of view, the larger standard deviation of the power level leads to more distinguishable power gradation, which benefits the estimation based on distance of power level. Likewise, a high power level means that the distance between a fingerprint point and an AP is small, which makes the user receiver more likely to receive as many APs as possible and this is good for achieving a high accuracy estimation.

However, as seen in Figures 5.6 and 5.7, the standard deviation is inversely proportional to the mean and median value of the heard power level. As a matter of fact, building 1 (Figure 5.6) has a better estimation accuracy than building 2 (Figure 5.7). Therefore, the standard deviation of heard APs power level per fingerprint point is inversely proportional to the estimation accuracy. Here, it seems we are trapped into a dilemma: the tradeoff between the high received signal strength and the distinguishable power level in a fingerprint point. Because the focus of this thesis is human mobility models and their behaviors under indoor technology, investigation on the deployment of APs here is general, the APs deployment will be no more discussed and left for the further study.

The above is the study of APs from the view of fingerprint points, which gives statistical description of APs deployment. The following shows the power maps of fingerprint. Figures 5.9(a), 5.9(b) and 5.9(c) show the fingerprints grid only with the power level heard from the 6th Access Point under 2 dB, 10 dB and 40 dB noise level respectively. Here for the cause of plotting the floor as a facet, the sign $*$ shows the position of AP seems on the second floor, but the $*$ is on the ceiling of the first floor and there is a wall between the 6th AP and second floor ground. Figures 5.9(d) and 5.9(e) show the power map and the fingerprint grid of the 16th and 212th APs, respectively.

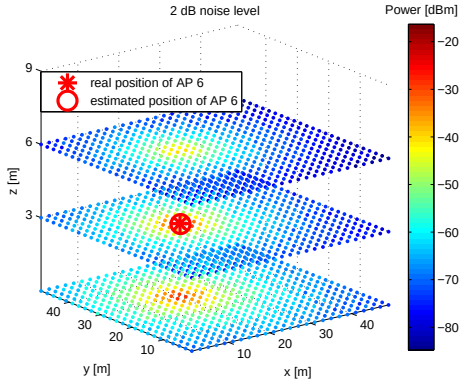

(a) Access Point 6 and corresponded power map (2 dB noise level-simulation)

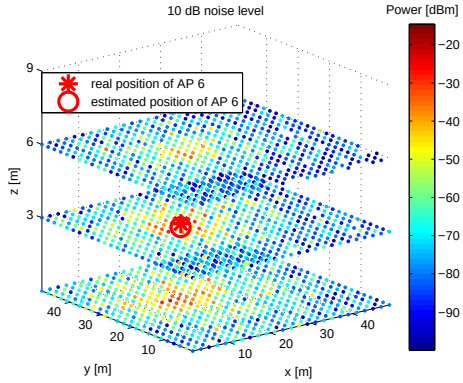

(b) Access Point 6 and corresponded power map (10 dB noise level-simulation)

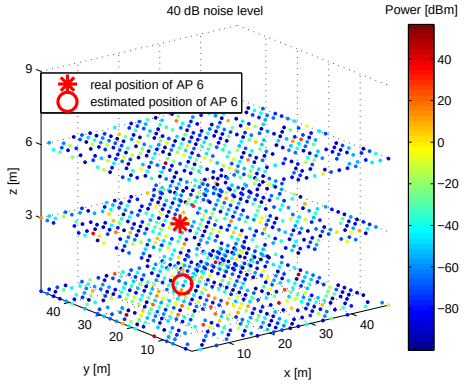

(c) Access Point 6 and corresponded power map (40 dB noise level-simulation)

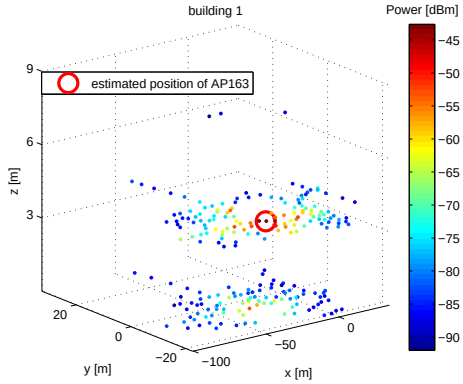

(d) Access Point 163 and corresponded power map (unknown noise level-building 1)

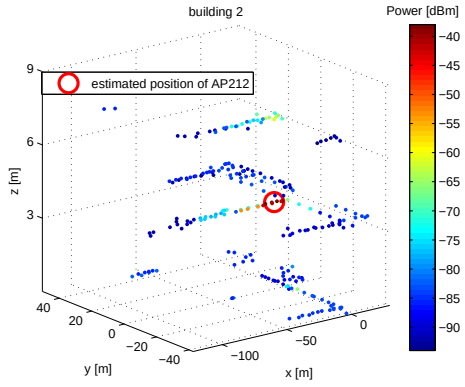

(e) Access Point 212 and corresponded power map (unknown noise level-building 2)

Figure 5.9: *One Access Point and corresponded power map. The $*$ represents the real position of the AP, the $\bigcirc$ represents the estimated position of AP. In Figure 5.9(a), Figure 5.9(b), Figure 5.9(c), Figure 5.9(d) and Figure 5.9(e), the position of the AP is estimated by eq.(5.2).*

In Figures 5.9(d) and 5.9(e), the position of the Access Point is estimated by sorting the fingerprint points position according to the power levels, then applying the equation below, N_n is the first n-th fingerprints positions after sorting (usually we let n equal to 4.):

$$(x_{ap}, y_{ap}, z_{ap}) = \sum_{i=1}^{N_n} \frac{P_i}{P_1 + \cdots + P_{N_n}} (x_i, y_i, z_i) \tag{5.2}$$

In eq. (5.2), regarding that the previous step the coordinates of fingerprint points are already sorted by the heard specific AP power level, we assume that the fingerprint point P_1 (x_1, y_1, z_1) has the maximum heard power level, P_2 (x_2, y_2, z_2) has the second maximum value and so forth. In practice, the value N_n is usually equal to 4 so that we can save amount of computing time. In this simulation, we let the value n equal to 4 and acquire the approximate coordinates of the 163rd AP and 212nd AP respectively.

5.3 Fingerprints setup

The fingerprints algorithm was introduced in Chapter 4. Here the principle of indoor fingerprints is not dwelled on, only the design details in this simulation is presented.

In Chapter 4, the eq. (4.1) was given to calculate the RSS of fingerprint points by applying classical path loss model with floor losses. The process to form the fingerprint was given in the same chapter. In this section, some specific issues related to the process talked above is discussed.

5.3.1 Floor loss

As it was mentioned in Section 4.4, due to the floor ground separating floors, the floor loss is introduced to describe this attenuation of signals power. In our simulator, we simply assume that the floor loss is constant and it is equal to 5 dB per floor for each time penetrating the floor ground. From Figures 5.9(a), 5.9(b) and 5.9(c), it is evident that the fingerprint points right under the 6th AP and as the same floor as the AP has larger power levels than the closest ones above the 6th AP but with a ceiling ground between them. This also points out that signals travelling in the air has less attenuation than penetrating the obstacles.

5.3.2 Fingerprint spacing

Speaking about the spacing among fingerprint points, there is always a tradeoff argument behind it. On one hand, when increasing the spacing between fingerprints, the accuracy is decreased, on the other hand, a decreased spacing brings higher computational complexity and it requires larger databases to be stored. Since the fingerprint grid in our simulator is two dimensional, only on the each floor ground, a small spacing is beneficial for both the computing and accuracy. Therefore the spacing is designed as 2 meters and the fingerprint grid is like in Figure 5.10(a), Figures 5.10(b) and 5.10(c) are presented here as a contrast to give a straightforward expression of different ways to design fingerprints spacing.

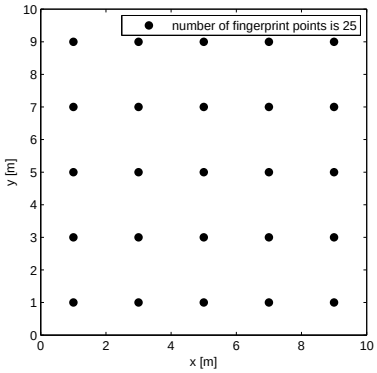

(a) 25 fingerprint points

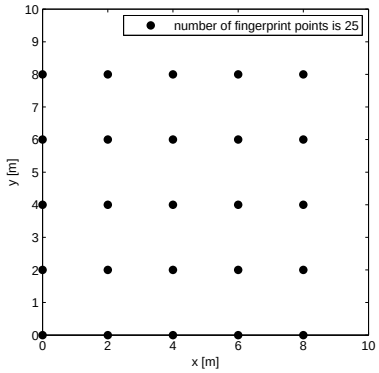

(b) 25 fingerprint points

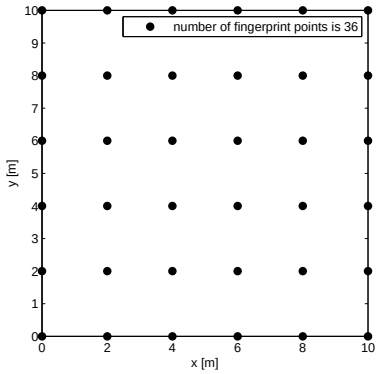

(c) 36 fingerprint points

Figure 5.10: *Some available fingerprint spacing examples, Figure 5.10(a) is the scheme used in this thesis, Figure 5.10(b) shares the same number of fingerprint points with Figure 5.10(a), the difference between Figures 5.10(a) and 5.10(b) is that when applying the estimation algorithm, in Figure 5.10(b), the right area near the boundary may not receive a good accuracy, 5.10(c) is another way to distribute fingerprint points. All these figures here are only for examples purpose, the optimization of fingerprint points spacing is not concerned in this thesis.*

5.4 Track formation

Practically, when users achieve indoor positioning service by applying fingerprint positioning technology, from users' point of view the most common parameter which users received is the changing RSS from various APs. In order to mimic this process, this section discuss the sampler which extracting data from chosen models and apply eq. (4.2) to build the track power level database.

5.4.1 Downsampling

In Chapter 3, to avoid simulation errors such as boundary ambiguity problem, the sampling rate was relative high and may lead to an enormous database size. For this reason it is however difficult to run the fingerprint method to test models. Down sampling is thus a necessary pretreatment before the formation of the track database.

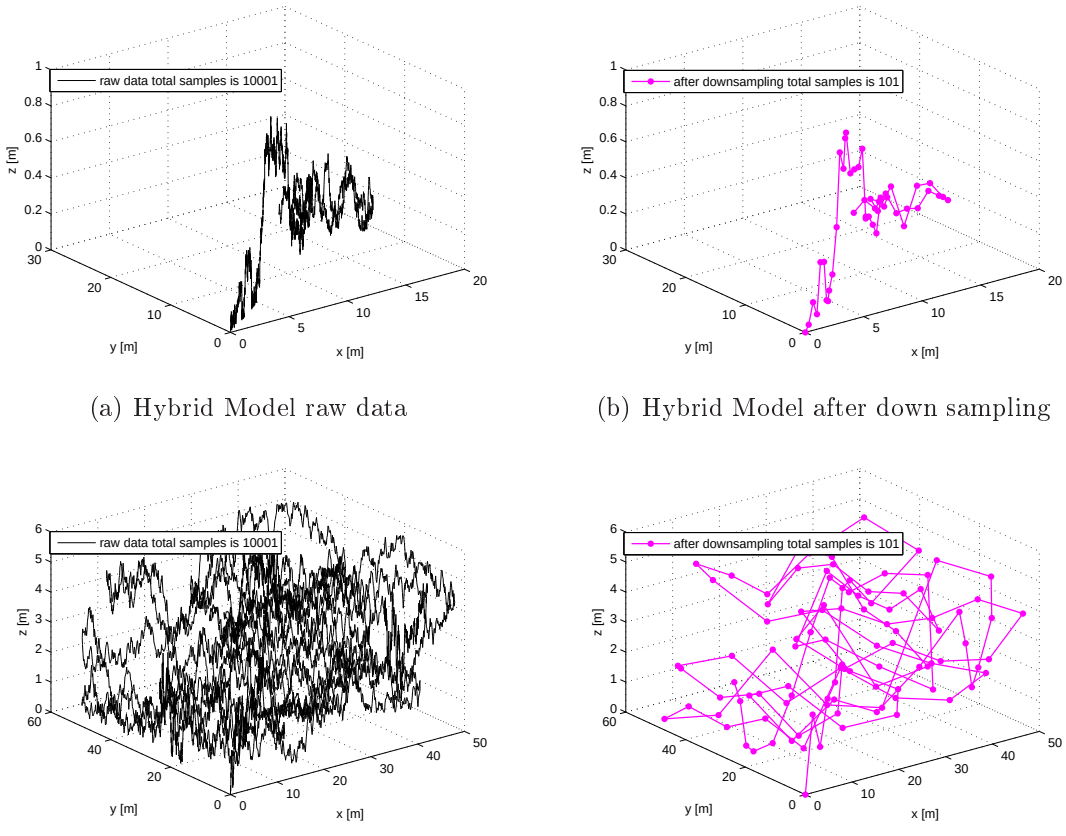

(a) Hybrid Model raw data

(b) Hybrid Model after down sampling

(c) Random Direction raw data

(d) Random Direction after down sampling

Figure 5.11: *One example to show down sampling principle. The number of used samples in figures is 10001.*

In the example shown in Figure 5.10, the downsampling rate is 100, meaning that 1 sample is kept from every 100 samples, and a total 7201 samples is collected for every one track. Figure 5.11(a) shows the raw data and correspondingly Figure 5.11(b) shows the data after down sampling. Similarly, Figures 5.11(c) and 5.11(d) show the raw data and the down sampling data respectively. The process with high sampling rate building data and down sampling the raw data, in a way, approaches the real scenarios and avoids distortedly description of human mobility patterns. The track database is generated based on the data after down sampling process.

5.4.2 Track database

The database is formed by applying eq. (4.2), with a 5 dB floor loss attenuation every time penetrating one floor ground. Inside the database it is organized as the Table 5.3.

Table 5.3: *Organization and design of tracks database*

Random Direction	**Hybrid Model**
40 tracks in total	40 tracks in total
= 2 velocity ranges	= 2 velocity ranges
× 4 starting points per velocity range	× 4 starting points per velocity range
× 5 tracks per starting point	× 5 tracks per starting point

In Chapter 3, the Random Direction Mobility Model and Hybrid Model are simply separated into two categories, the small range velocity and the large range velocity. By doing so we assume the possibility that the different velocity range significantly influences the mobile behavior in the fingerprint method. And this assumption will be testified in the Chapter 6.

Besides, '4 starting points' are used to test the effect of various starting points on the accuracy of fingerprint positioning method. '5 tracks' are used to provide average statistics in order to mitigate bias approximation. In Chapter 6, one more comparison like noise power level is also added.

5.5 Summary

In this chapter, we started with a discussion on Access Point deployment. The method discussed in this chapter is simply used to give a general idea about the feasibility of APs deployment. Meantime, two real-field data collected from building 1 and building 2 were introduced as a reference to evaluate APs deployment in the

simulation. As an observation result from the two set of real-field data, the standard deviation of heard APs power level per fingerprint point is inversely proportional to the power level of heard APs per fingerprint point. Therefore it is concluded there is probably a tradeoff between standard deviation of heard APs power level per fingerprint point and power level of heard APs per fingerprint point. Again, this observation is not the main focus of the thesis, but it is a good beginning for the future indoor positioning study.

Later in this chapter, some details such as floor loss and spacing were discussed, the formation of track database was introduced as well.

Through Figures 5.9(a), 5.9(b) and 5.9(c), it was quite obvious to see the effect of adding floor loss in the simulation. The spacing issue was talked by demonstrating 3 figures with different distribution of fingerprint points; the merits and demerits were not discussed here. The APs deployment and fingerprint grid were only for the testing purpose; once these are set up, they remain the same and are used for all the test.

The database of user tracks was organized as shown in Table 5.3, through 3 velocity ranges and 4 starting points. '5 tracks per starting point' was used for the purpose of a less biased approximation.

6. SIMULATION-BASED RESULTS

6.1 Gaussian likelihood estimation

In the Chapter 4 we talked about Gaussian likelihood function, and we gave the expression to calculate it. The Gaussian likelihood method, in other words, is a probabilistic way to describe the distance between two power levels and at the same time, taking into account the background noise. The Gaussian likelihood method is the best way to implement the power level distance estimation. Figures 6.1(a), 6.1(b) and 6.1(c) show three alternatives that could use to estimate positions, the algorithm uses eq. (6.2), others see eq. (6.1) and (6.3).

In the Figure 6.1, all the algorithm are based on Gaussian likelihood. Among them the principle of algorithm 1 is eq. (6.1), algorithm 2 is eq. (6.2) and algorithm 3 is eq. (6.3).

$$L_1 = \sum_{heard\ ap} \left(\frac{1}{\sqrt{2\pi\sigma_{ap}^2}} e^{\frac{\left(R_{ap}-P_{i,ap}\right)^2}{2\sigma_{ap}^2}} \right) \tag{6.1}$$

$$L_2 = \sum_{heard\ ap} \log_{10} \left(\frac{1}{\sqrt{2\pi\sigma_{ap}^2}} e^{-\frac{\left(R_{ap}-P_{i,ap}\right)^2}{2\sigma_{ap}^2}} \right) \tag{6.2}$$

$$L_3 = \sum_{heard\ ap} \left(\frac{1}{\sqrt{2\pi\sigma_{ap}^2}} e^{\frac{\left(R_{ap}-P_{i,ap}\right)^2}{2\sigma_{ap}^2}} \right) |R_{ap} - P_{i,ap}| \tag{6.3}$$

Obviously, it can be seen from Figure 6.1, the algorithm 2 is the best amongst them.

6.2 Root mean square error

Root Mean Square Error (RMSE) is commonly to evaluate the behavior of estimation algorithms. From Section 6.1, we get the estimated position $(\hat{x}, \hat{y}, \hat{z})$ which

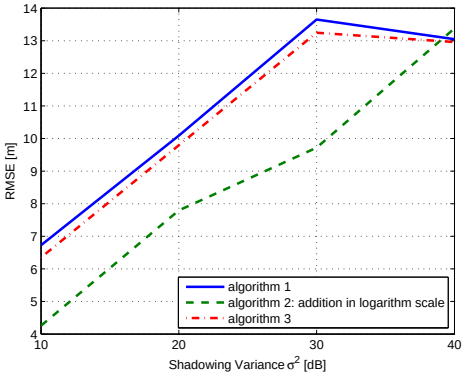

(a) Hybrid Model with 3 algorithms

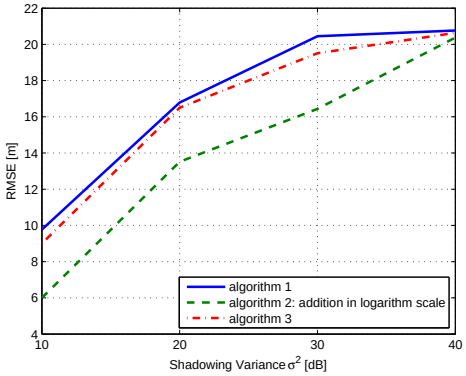

(b) Random Direction with 3 algorithms

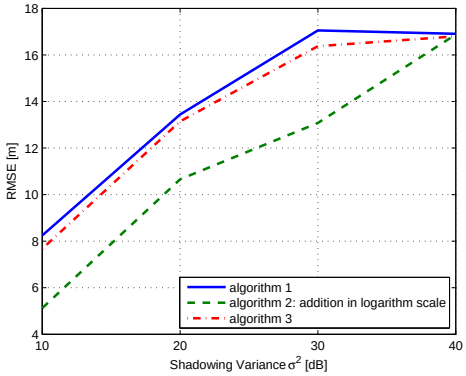

(c) Average of two models with 3 algorithms

Figure 6.1: *Comparison among three estimation algorithms. The range of noise power level is 10 dBm - 40 dBm.*

maximizes the Gaussian likelihood. Then the RMSE value of distance between the real location and the estimated one can be expressed as follow:

$$RMSE = \sqrt{mean\Big(\sum_{i=1}^{n}\big((x_i - \hat{x}_i)^2 + (y_i - \hat{y}_i)^2 + (z_i - \hat{z}_i)^2\big)\Big)} \tag{6.4}$$

From Section 5.4.2, the true location is known in the RMSE computation. It is assumed that the noise variance of APs keeps constant for each test.

Due to the lack of human mobility data collected in real life, based on Figure 6.2 it is concluded that the Hybrid Model has a better estimation accuracy than the Random Direction Mobility Model under fingerprint algorithm and Bayesian estimation. The most likely reason for this better accuracy is the uneven distribution of mobile positions in Hybrid Model.

From Figure 6.2, there are no differences among different starting points and dif-

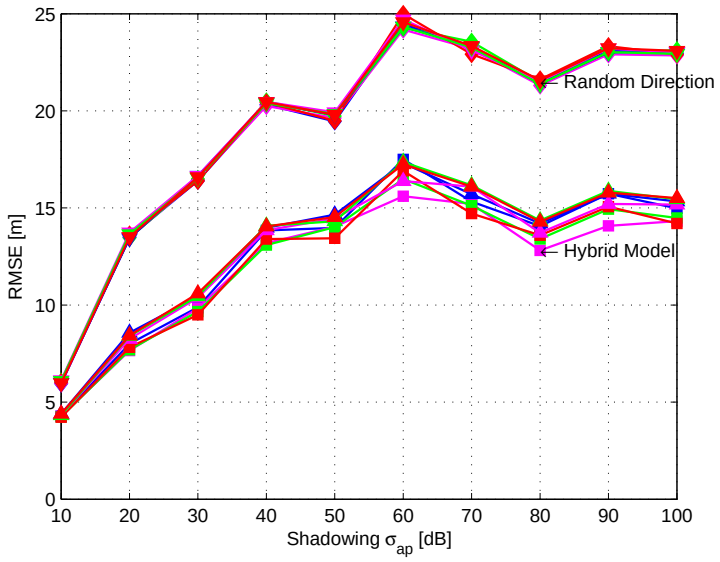

Figure 6.2: *RMSE versus Noise variance.*
In the upper group lines they are RMSE values of estimation using Random Direction Mobility Model, in the lower group lines they are RMSE values of estimation using Hybrid Model. In both these two group lines, there are 4 starting points and 2 velocity ranges.

ferent velocity ranges. Figure 6.3 shows the variation of RMSE value when only one parameter changes. By comparing Figure 6.3(a) with Figure 6.3(b) and Figure 6.3(c) with Figure 6.3(d), we see that the different velocity range barely influences the RMSE value. By looking at any curve in Figure 6.3, we can see that the diverse starting points make negligible difference to the RMSE value. By looking at Figure 6.2 we could summarize that the Hybrid Model is slightly sensitive to velocity range. The cause of this might be the uneven distribution issue mentioned before.

In addition, from Figure 6.4 it is clear to see the influence of environment noise in the RMSE value. Under 10 dB noise condition, the Random Direction Mobility Model can acquire around 5 meter accuracy with 0.8 probability, and the Hybrid Model can achieve even higher probability (0.9). However, in the 40 dB noise situation, it is very difficult for both these two models to achieve relative high accuracy with fair probability.

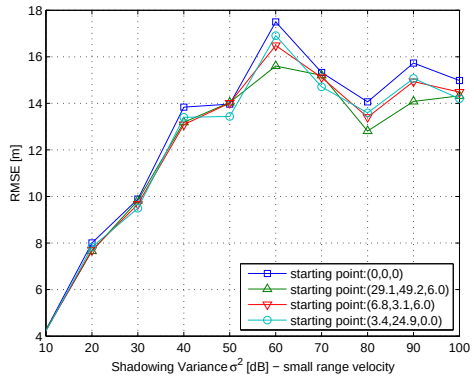

(a) Hybrid Model with small velocity range

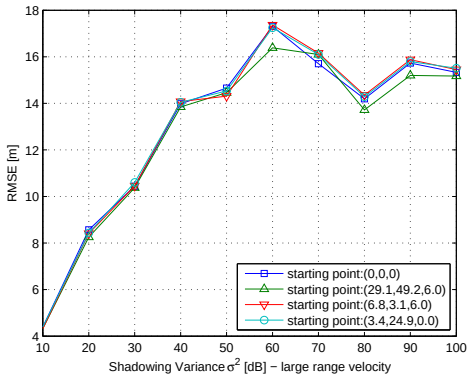

(b) Hybrid Model with large velocity range

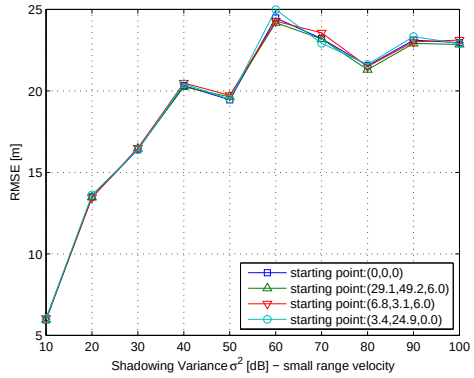

(c) Random Direction with small velocity range

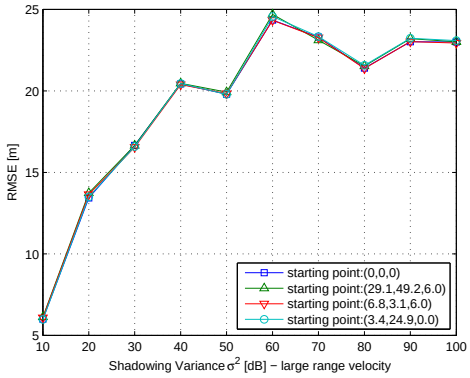

(d) Random Direction with large velocity range

Figure 6.3: *RMSE value versus noise level. 4 starting points and 2 velocity range.*

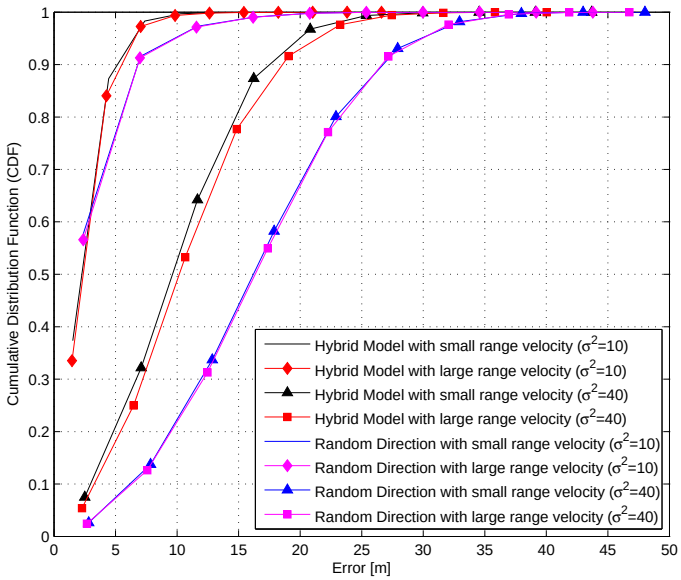

Figure 6.4: *RMSE versus Noise. Only 10 dB noise level and 40 dB noise level are given, which represent the moderate noise level and upper limit noise level.*

To sum up, first of all, the impact of velocity range and starting point on the positioning accuracy (i.e., the RMSE value under fingerprint algorithm and Bayesian estimation) can be neglected. Secondly, compared with the Random Direction Mobility Model, the Hybrid Model has better positioning accuracy but it is slightly sensitive to the velocity range. Last but not least, the environmental noise power level is crucial to the positioning accuracy and the type of mobility models plays an important role in the positioning accuracy.

7. BRIEF STUDY ABOUT VELOCITY AND ANGLE DEPENDENCIES ON RSS

This chapter is the result of an open-end research so far and it aims at exploring the properties of RSS and their relationship to the human mobility parameters. In the current work, when applying fingerprint algorithm we build connection between RSSs of that moment and the position information. However, due to the extremely frequent slow movement of human beings inside a space (i.e., office, home etc...), the velocity is in an actual slow-changing process. Thus, the prediction of the next move based on historical movements is possible. Therefore the discussion in this chapter describes a picture of this thought and it gives the conclusions until now.

To start with, the research includes two different directional ways of exploration:

1. Finding the relationship between the velocity and power changing characteristics;

2. Using the relationship found in step 1 to predict the current position by comparing and analysing the power received now and before.

Table 7.1 shows the design of the velocity part, and Table 7.2 shows the design of the angle part.

Under these design, if we consider a noise free space, the simulation result of velocity is illustrated in Figure 8.1:

From Figure 7.1(c), it can be concluded that the velocity has impact on the rate of power level change. From Figure 7.1(c), we can see that the peak value is the same no matter what the speed is. The velocity parameter determines the time which is needed by the power level of the mobile to return its starting power level.

Similarly, by following the design in Table 7.2 and assuming noise free simulation

[15] In the Figure 7.1, we simply take values from 0.80 to 1.10 with 0.05 step [unit: m].
[16] In the Figure 7.2, we take values from 0 to $\pi/2$ with $\pi/8$ step [unit: rad].

Table 7.1: *Velocity simulation design*

Parameter	**Value**
simulation area	10×10 2-D [m]
number of AP	1
AP power	0 [dBm]
AP location	(5,5) [m]
path loss coefficient	n_{ap}=2
noise	to be defined (Gaussian distribution)
angle	$\pi/4$ [rad]
velocity	0.89-1.08[15] [m/s]
sampling frequency	10 [Hz]
track	from (0,0) to (10,10) straight [m]
fingerprint	spacing=0.2 [m]

Table 7.2: *Angle simulation design*

Parameter	**Value**
simulation area	10×10 2-D [m]
number of AP	1
AP power	0 [dBm]
AP location	(5,5) [m]
path loss coefficient	n_{ap}=2
noise	to be defined (Gaussian distribution)
angle	0-$\pi/2$[16] [rad]
velocity	0.9 [m/s]
sampling frequency	10 [Hz]
fingerprint	spacing=0.2 [m]

space, the simulation result figures of angle is given in Figure 8.1. In Figures 7.2(a), 7.2(b), 7.2(c), 7.2(d) and 7.2(e), the blue line represents the track and the green line represents the changing power along with the change of the mobile position.

From Figure 7.2(g), we comprehend that the angle not only determine the peak value of power level plot but also the time which is needed for power level curve return to its starting value. If the simulated area is fixed, there is non-zero probability that in the angle case the power level curve may not return to its starting value. In this sense, the angle parameter mainly determine the peak value.

In brief, the velocity is strongly related to the time which is needed for the power curve to return to its starting value. The angle is crucial to the peak value of the power level curve.

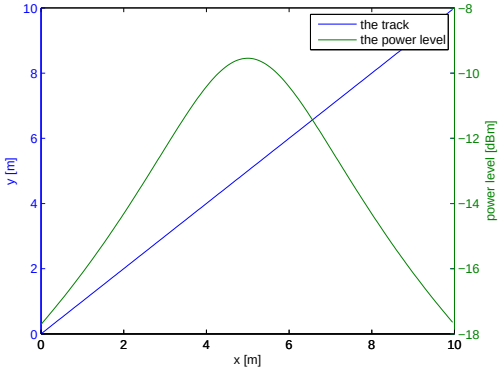

(a) Track and Power changes with distance

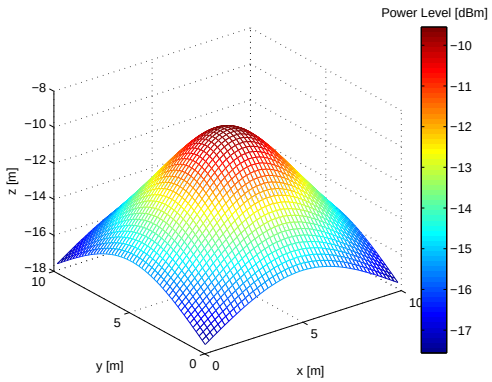

(b) Fingerprint power grid

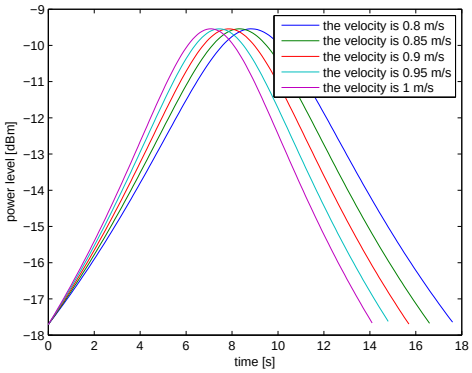

(c) Comparison among velocities

Figure 7.1: *Velocity study under noise free condition. In the Figure 7.1(a), the blue line represents the track and the green line represents the changing power along with the change of the mobile position. Figure 7.1(b) is the fingerprint power grid. Figure 7.1(c) lists all the results in this simulation, received power level changes with the various velocities. *note: transmitted power is 0 dBm.*

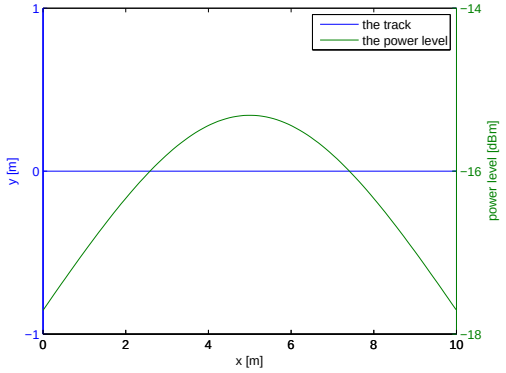

(a) The angle is 0

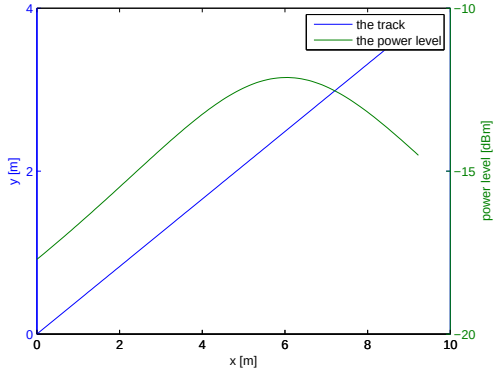

(b) The angle is $\pi/8$

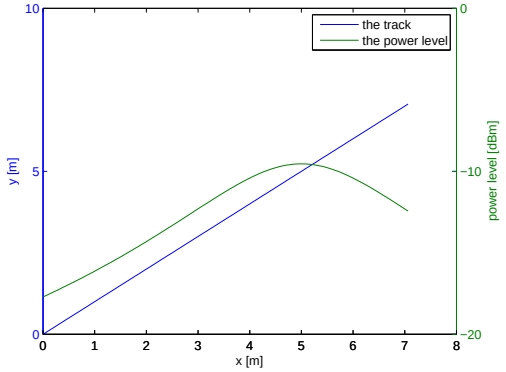

(c) The angle is $\pi/4$

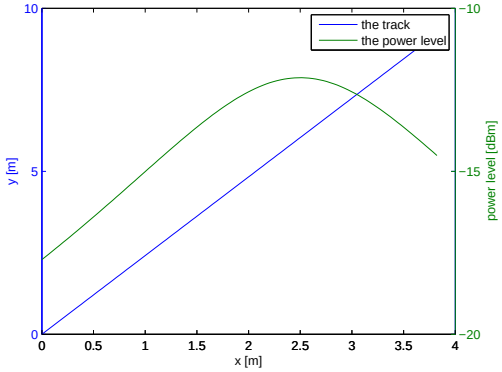

(d) The angle is $3\pi/8$

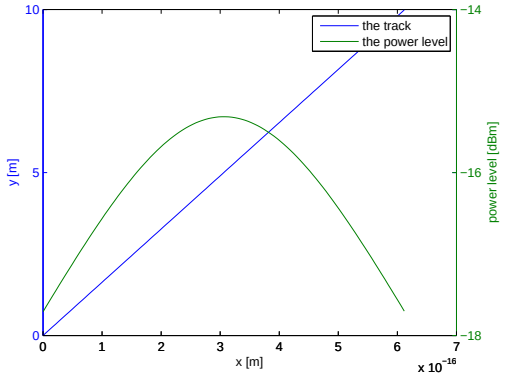

(e) The angle is $\pi/2$

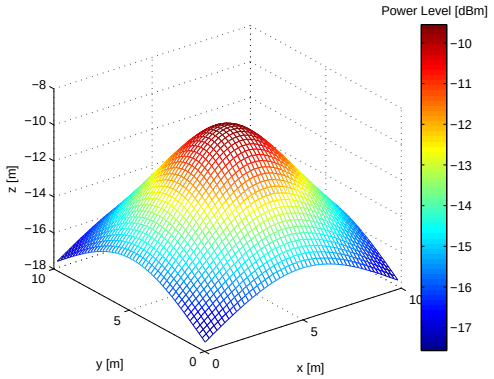

(f) Fingerprint power grid

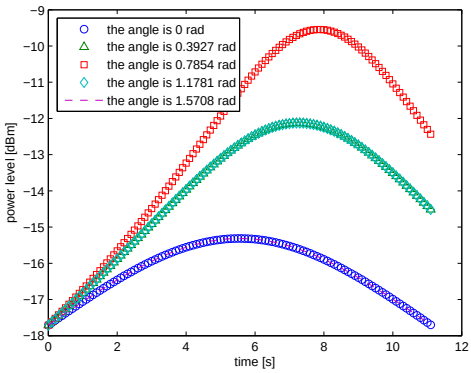

(g) Comparison among angles, the upper and lower one are overlapped

Figure 7.2: *Angle study under noise free condition. *note: transmitted power is 0 dBm.*

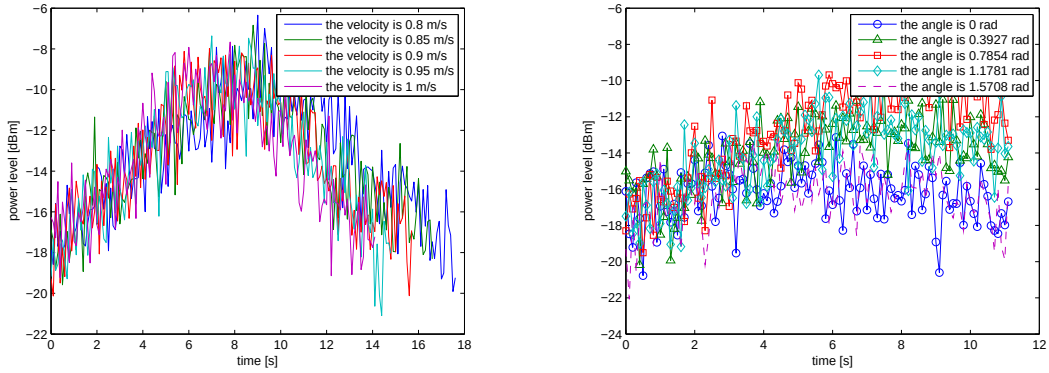

(a) Velocity study (under noise)

(b) Angle study (under noise)

Figure 7.3: *Velocity and angle study under slight noise power [2 dB] level *note: transmitted power is 0 dBm.*

Figures 7.3(a) and 7.3(b) shows the power level curves versus the variation of the velocity and the angle respectively. The conclusion we made from the noise free case may not be solid when the conclusion is applied to the 2 dB noise power level case. Even a low noise level rather destroys these nice characteristics and more investigation is needed to draw universal conclusions on the RSS relationship with angles and directions.

8. DESIGN RECOMMENDATION

As it was said in the Introduction chapter, considering the uplink and downlink in the wireless network, the influence between the user devices and the access points is mutual. The movements of users affects the way the mobile receives and transmits the signals. The study of human mobility patterns not only makes contribution to indoor positioning but it also benefits the research of wireless network. All of these motivate us to push the study of human mobility patterns forward.

8.1 Complexity and suitability for real-life scenarios

Speaking of human mobility models, it is inevitable to discuss the compromise between how complex the models could be and in what degree the models could describe real scenarios.

One priority of indoor positioning system is low complexity, which is the precondition of its popularity. Due to many description of human mobility characterization, the Hybrid Model has higher complexity than the Random Direction Mobility Model. This is the main disadvantage of the Hybrid Model.

The Hybrid Model coexists with the Random Direction Mobility Model, because even if the movements of most people inside a building are closer to Hybrid Model, there still are minor cases such as the cleaner inside a building. So under this consideration, multiple models are needed to approach the detailed description of indoor human mobility patterns. And the unity of diverse models seems unlikely for now.

8.2 Future challenges and opportunities

The indoor positioning has many challenges now. Positioning is like most other cutting edge technologies, that people did not realize its potential conflict with ethic issues before it was born. While the concept of indoor positioning is fashionable, people learned from GNSS positioning technologies that positioning has possibility

to violate privacy issues etc. This obscurely brings obstruction to the development of indoor positioning technologies, for example, collecting movements data of human beings from real life usually is impossible or at least difficult. Besides, unlike the satellite based positioning, in the indoor positioning area the indoor positioning technology does not have universal standard until now. The status quo of this area is still lab work [33, 32] or business release [42, 19, 20] within a small scale. Most indoor positioning projects are business oriented work rather than government leading projects. This is another reason why the universal standard of indoor positioning technologies is not yet formed.

In the meantime, we should also have faith in the future of indoor positioning technologies. With the increasing requirement of Location-based Service (LBS), people will eventually move their focus from outdoor positioning to the indoor positioning. In addition, as a common sense, office people stay longer inside a building rather than outside it, firemen extinguish fire mostly inside a building etc. These facts motivate the indoor positioning technology to make a move forward.

Table 8.1: *Challenges and opportunities*

Challenges	**Opportunities**
ethical issues in collecting data for human mobility models	positioning algorithms enhanced with predictive engines based on human mobility patterns
need of huge data collection for statistically significant results	developing standards for indoor positioning

8.3 Future studies

The indoor scenarios are complex, one or two indoor human mobility models cannot precisely describe every patterns of human mobility under indoor environment. Thus the indoor human mobility models still need to be developed. For example, a human mobility model inside a supermarket.

In this thesis, the spacing between fingerprints are large, which limits the accuracy of positioning. A method to decrease the spacing between fingerprints and meantime to increase much computation is under development. Recently there are many research on the prediction of human mobility, and in this way the size of fingerprint grid may be decreased. This idea gives an alternative to increase the accuracy and not to bring too much burden to the computation.

9. CONCLUSIONS

This thesis work presented a investigation of current popular human mobility models, proposed a novel model namely Hybrid Model for indoor positioning study and tested the suitable models (i.e., Random Direction Mobility Model and Hybrid Model) with fingerprint algorithm and Bayesian estimation for the purpose of indoor positioning. In addition, this thesis also briefly investigated the relationships between the movement direction changes and speeds to the Received Signal Strength fluctuations.

Chapter 1 started with the introduction of the background of this thesis work, then the author's contribution and organization of this thesis was listed. In Chapter 2, we reviewed the current fashionable indoor positioning technologies and commented each technology from the point of view of the feasibility and cost. In Chapter 3, Random Walk Mobility, Random Waypoint Mobility Model, Random Direction Mobility Model and Boundless Simulation Area Mobility Model were introduced together with a discussion on their feasibility in indoor scenarios. Then the proposed model, which is used to specifically describe office movements of human beings, was given and discussed. In Chapter 3, the details on how to form the above models and the characterization of Hybrid Model were also included. In Chapter 4, we talked about various traits of indoor environment and then we explained the assumptions used in the Random Direction Mobility Model and the Hybrid Model. Then, the classical path loss model was briefly expressed. Finally, the fingerprint process and the estimation methods were explained. In Chapter 5, the deployment of Access Points was detailed and particularly one possible evaluation method of APs setup was introduced there. A method about the relationship between the AP density and the positioning accuracy was also introduced. Later on, the fingerprint setup and the track formation were presented. In this track formation section, the downsampling concept was discussed by comparing Figure 5.11(a) with Figure 5.11(b) (or Figure 5.11(c) with Figure 5.11(d)). In Chapter 6, it was concluded that, under the fingerprint algorithm and the Bayesian estimation, the Hybrid Model has a better positioning accuracy than the Random Direction Mobility Model. We also showed that parameters such as velocity range and the starting point have only a tiny impact on the positioning accuracy (in the thesis, the accuracy is characterized

in terms of the Root Mean Square Error value). In Chapter 7 and 8, the challenges and opportunities in the indoor positioning area were discussed, and at the same time, part of the current work is briefly introduced to give the readers a general idea about future work in this area.

BIBLIOGRAPHY

[1] "Active bat," http://www.cl.cam.ac.uk/research/dtg/attarchive/bat/, Apr. 2015.

[2] "Ekahau," http://www.ekahau.com/, Apr. 2015.

[3] "Sonitor system," http://www.sonitor.com/, Apr. 2015.

[4] "Ubisense," http://www.ubisense.net/, Apr. 2015.

[5] "World record," http://www.digplanet.com/wiki/List_of_world_records_in_athletics, Apr. 2015.

[6] G. Almes, S. Kalidindi, A. Morton, and M. Zekauskas, "A one-way delay metric for ippm," 2014.

[7] K. Aspelin, "Establishing pedestrian walking speeds," http://www.westernite.org/datacollectionfund/2005/psu_ped_summary.pdf, Apr. 2015.

[8] P. Bahl and V. N. Padmanabhan, "Radar: An in-building rf-based user location and tracking system," in *INFOCOM 2000. Nineteenth Annual Joint Conference of the IEEE Computer and Communications Societies. Proceedings. IEEE*, vol. 2, Mar. 2000, pp. 775–784.

[9] A. Basiri, E. S. Lohan, P. F. e Silva, P. Peltola, C. Hill, and T. Moore, "Overview of positioning technologies from fitness-to-purpose point of view," in *Localization and GNSS (ICL-GNSS), 2014 International Conference on. IEEE*, Jun. 2014, pp. 1–7.

[10] C. Boake, S. R. McCauley, H. S. Levin, C. Pedroza, C. F. Contant, J. X. Song, S. A. Brown, H. Goodman, S. I. Brundage, and P. J. Diaz-Marchan, "Diagnostic criteria for postconcussional syndrome after mild to moderate traumatic brain injury," 2014.

[11] B. Brumitt, B. Meyers, J. Krumm, A. Kern, and S. Shafer, "Easyliving: Technologies for intelligent environments," in *Handheld and ubiquitous computing*. Springer, 2000, pp. 12–29.

[12] T. Camp, J. Boleng, and V. Davies, "A survey of mobility models for ad hoc network research," *Wireless communications and mobile computing*, vol. 2, no. 5, pp. 483–502, 2002.

[13] J. J. Collins and C. J. D. Luca, "Open-loop and closed-loop control of posture: a random-walk analysis of center-of-pressure trajectories," *Experimental brain research*, vol. 95, no. 2, pp. 308–318, 1993.

[14] R. Fei, B. Hu, R. Ma, and L. Wang, "Formulation and analysis of mobility points based the semi-markov model," in *Natural Computation (ICNC), 2013 Ninth International Conference on.* IEEE, 2013, pp. 1579–1584.

[15] D. Focken and R. Stiefelhagen, "Towards vision-based 3-d people tracking in a smart room," in *Multimodal Interfaces, 2002. Proceedings. Fourth IEEE International Conference on.* IEEE, 2002, pp. 400–405.

[16] B. Gloss, M. Scharf, and D. Neubauer, "Location-dependent parameterization of a random direction mobility model," in *Vehicular Technology Conference, 2006. VTC 2006-Spring. IEEE 63rd*, vol. 3. IEEE, 2006, pp. 1068–1072.

[17] M. C. Gonzalez, C. A. Hidalgo, and A. L. Barabasi, "Understanding individual human mobility patterns," *Nature*, vol. 453, no. 7196, pp. 779–782, 2008.

[18] Y. Gu, A. Lo, and I. Niemegeers, "A survey of indoor positioning systems for wireless personal networks," *Communications Surveys & Tutorials, IEEE*, pp. 13–32, Nov. 2009.

[19] A. Harter and A. Hopper, "A distributed location system for the active office," *Network, IEEE*, vol. 8, no. 1, pp. 62–70, 1994.

[20] A. Harter, A. Hopper, P. Steggles, A. Ward, and P. Webster, "The anatomy of a context-aware application," *Wireless Networks*, vol. 8, no. 2/3, pp. 187–197, 2002.

[21] J. Hightower, R. Want, and G. Borriello, "Spoton: An indoor 3d location sensing technology based on rf signal strength," *UW CSE 00-02-02, University of Washington, Department of Computer Science and Engineering, Seattle, WA*, vol. 1, 2000.

[22] C. Interactive, "Firefly motion capture system," http://www.cybernet.com/interactive/firefly/index.html, Apr. 2015.

[23] D. B. Johnson and D. A. Maltz, "Dynamic source routing in ad hoc wireless networks," in *Mobile computing.* Springer, 1996, pp. 153–181.

[24] T. King, S. Kopf, T. Haenselmann, C. Lubberger, and W. Effelsberg, "Compass: A probabilistic indoor positioning system based on 802.11 and digital

compasses," in *Proceedings of the 1st international workshop on Wireless network testbeds, experimental evaluation & characterization.* ACM, 2006, pp. 34–40.

[25] J. Krumm, S. Harris, B. Meyers, B. Brumitt, M. Hale, and S. Shafer, "Multi-camera multi-person tracking for easyliving," in *Visual Surveillance, 2000. Proceedings. Third IEEE International Workshop on.* IEEE, 2000, pp. 3–10.

[26] B. Liang and Z. J. Haas, "Predictive distance-based mobility management for pcs networks," in *INFOCOM'99. Eighteenth Annual Joint Conference of the IEEE Computer and Communications Societies. Proceedings. IEEE*, vol. 3. IEEE, 1999, pp. 1377–1384.

[27] H. Liu, H. Darabi, P. Banerjee, and J. Liu, "Survey of wireless indoor positioning techniques and systems," *Systems, Man, and Cybernetics, Part C: Applications and Reviews, IEEE Transactions on*, vol. 37, no. 6, pp. 1067–1080, 2007.

[28] S. Misra, J. Mahapatro, M. Mahadevappa, and N. Islam, "Random room mobility model and extra-wireless body area network communication in hospital buildings," *IET Networks*, vol. 4, no. 1, pp. 54–64, 2014.

[29] W. Navidi and T. Camp, "Stationary distributions for the random waypoint mobility model," *Mobile Computing, IEEE Transactions on*, vol. 3, no. 1, pp. 99–108, 2004.

[30] H. Nurminen, J. Talvitie, S. Ali-Loytty, P. Muller, E. S. Lohan, R. Piché, and M. Renfors, "Statistical path loss parameter estimation and positioning using rss measurements," in *Ubiquitous Positioning, Indoor Navigation, and Location Based Service (UPINLBS), 2012.* IEEE, 2012, pp. 1–8.

[31] V. Paelke and C. Reimann, "Vision-based interaction-a first glance at playing mr games in the real-world around us," in *Proceedings of the 2nd International Workshop on Pervasive Gaming Applications (PerGames) at ERVASIVE*, vol. 2005, 2005.

[32] N. B. Priyantha, "The cricket indoor location system," Ph.D. dissertation, Massachusetts Institute of Technology, 2005.

[33] N. B. Priyantha, A. Chakraborty, and H. Balakrishnan, "The cricket location-support system," in *Proceedings of the 6th annual international conference on Mobile computing and networking.* ACM, 2000, pp. 32–43.

[34] K. C. Roberts, M. Shields, M. de Groh, A. Aziz, and J. A. Gilbert, "Overweight and obesity in children and adolescents: results from the 2009 to 2011 canadian health measures survey," *Health Rep*, vol. 23, no. 3, pp. 37–41, 2012.

[35] E. M. Royer, P. M. Melliar-Smith, and L. E. Moser, "An analysis of the optimum node density for ad hoc mobile networks," in *Communications, 2001. ICC 2001. IEEE International Conference on*, vol. 3. IEEE, 2001, pp. 857–861.

[36] Z. Ruxin, G. Fei, and Y. Jie, "Nonuniform property of random direction mobility model for manet," in *Wireless Communications, Networking and Mobile Computing, 2009. WiCom'09. 5th International Conference on.* IEEE, 2009, pp. 1–4.

[37] M. Sánchez and P. Manzoni, "Anejos: a java based simulator for ad hoc networks," *Future generation computer systems*, vol. 17, no. 5, pp. 573–583, 2001.

[38] S. Shrestha, J. Talvitie, and E. S. Lohan, "Deconvolution-based indoor localization with wlan signals and unknown access point locations," in *Localization and GNSS (ICL-GNSS), 2013 International Conference on.* IEEE, 2013, pp. 1–6.

[39] J. Talvitie, E. S. Lohan, and M. Renfors, "The effect of coverage gaps and measurement inaccuracies in fingerprinting based indoor localization," in *Localization and GNSS (ICL-GNSS), 2014 International Conference on.* IEEE, 2014, pp. 1–6.

[40] I. TranSafety, "Study compares older and younger pedestrian walking speeds," http://www.usroads.com/journals/p/rej/9710/re971001.htm, Apr. 2015.

[41] T. Wang and C. P. Low, "Determine the inter-arrival time in the non-uniform random waypoint mobility model," in *Wireless Days (WD), 2010 IFIP.* IEEE, 2010, pp. 1–5.

[42] R. Want, A. Hopper, V. Falcao, and J. Gibbons, "The active badge location system," *ACM Transactions on Information Systems (TOIS)*, vol. 10, no. 1, pp. 91–102, 1992.

[43] A. Ward, A. Jones, and A. Hopper, "A new location technique for the active office," *Personal Communications, IEEE*, vol. 4, no. 5, pp. 42–47, 1997.

[44] M. A. Youssef, A. Agrawala, and A. U. Shankar, "Wlan location determination via clustering and probability distributions," in *Pervasive Computing and Communications, 2003.(PerCom 2003). Proceedings of the First IEEE International Conference on.* IEEE, 2003, pp. 143–150.

APPENDIX A. RANDOM DIRECTION MOBILITY MODEL SIMULATOR

The full version of Matlab simulators used in this thesis will be available at

`http://www.cs.tut.fi/tlt/pos/Software.htm` after September 2015.

```
%%%%%%%%%%%%%%%%%%%%%%%%%%%%%%%%%%%%%%%%%%%%%%%%%%%%%%%%%%%%%%%%%%%%%%%%%%%%
%                                                                              %
%       Department of Electronics and Communication Engineering                %
%                          WANG WENBO - 238970                                 %
%                                                                              %
%                  random direction mobility model                            %
%                                                                              %
%%%%%%%%%%%%%%%%%%%%%%%%%%%%%%%%%%%%%%%%%%%%%%%%%%%%%%%%%%%%%%%%%%%%%%%%%%%%

close all;
clear all;
clc;

%% variables
% define x-y plane
xmax=50;ymax=50;

% simulation time
%N=10*60*600;
N=5e3;

% the number of floors
noOfFloor=3;

% the height spacing of floors
floorHeight=3;

%starting point

%{
```

```
x0=0;y0=0;z0=0;
%}

temp_3=0:floorHeight:floorHeight*(noOfFloor-1);

%{
x0=xmax*rand;
y0=ymax*rand;
z0=temp_3(randi(length(temp_3)));
%}

% loading predefined starting point
load('para2.mat');

% sampling frequency
Fs=10;
t=1/Fs;

% velocity interval
v_max=3;v_min=0.5;
%v_min=0.89;v_max=1.083;

% generate velocity variables using setVariable function
v=setVariable(v_min,v_max,'normal',N);

% displacement per time [m]
d=v*t;

zmin=0;zmax=(noOfFloor-1)*floorHeight;

%%{
%% 2-D
figure;

%hOut = inout.output();
%hOut.figure;

% plot the boundary
h4=plot([0 xmax],[ymax ymax],'r-','linewidth',1.5); hold on;
```

```
plot([0 xmax],[0 0],'r-','linewidth',1.5);
plot([0 0],[0 ymax],'r-','linewidth',1.5);
plot([xmax xmax],[0 ymax],'r-','linewidth',1.5);

% process
trace(1,1)=x0;
trace(2,1)=y0;

% direction
r=-pi+2*pi*rand;

count=1;

for n=1:N

    % starting point
    h1=plot(x0,y0,'go','markersize',10,'linewidth',1.5);grid on;

    % set axis scale
    axis('square',[-5 xmax+5 -5 ymax+5]);

    trace(1,count+1)=trace(1,count)+d(n)*cos(r);
    trace(2,count+1)=trace(2,count)+d(n)*sin(r);

    % if, elseif and else are used to determine if the user cross the boundary
    if trace(1,count+1)<xmax&&trace(1,count+1)>0&&trace(2,count+1)<ymax&&...
    trace(2,count+1)>0
        plot(trace(1,count:count+1),trace(2,count:count+1),'k-',...
        'linewidth',0.6);
        count=count+1;
    elseif trace(1,count+1)>xmax&&trace(2,count+1)<0
        trace(1,count+1)=xmax;
        trace(2,count+1)=0;
        plot([trace(1,count),xmax],[trace(2,count),0],'k-','linewidth',0.6);
        plot(xmax,0,'ko','markersize',5,'markerface','k');
        count=count+1;
        r=setVariable(pi/2,pi,'normal',1);
        trace(1,count+1)=xmax+d(n)*cos(r);
        trace(2,count+1)=d(n)*sin(r);
```

```
        plot([xmax,trace(1,count+1)],[0,trace(2,count+1)],'k-','linewidth',0.6);
        count=count+1;
    elseif trace(1,count+1)>xmax&&trace(2,count+1)>ymax
        trace(1,count+1)=xmax;
        trace(2,count+1)=ymax;
        plot([trace(1,count),xmax],[trace(2,count),ymax],'k-','linewidth',0.6);
        plot(xmax,ymax,'ko','markersize',5,'markerface','k');
        count=count+1;
        r=setVariable(pi,3*pi/2,'normal',1);
        trace(1,count+1)=xmax+d(n)*cos(r);
        trace(2,count+1)=ymax+d(n)*sin(r);
        plot([xmax,trace(1,n+1)],[ymax,trace(2,n+1)],'k-','linewidth',0.6);
        count=count+1;
    elseif trace(1,count+1)<0&&trace(2,count+1)>ymax
        trace(1,count+1)=0;
        trace(2,count+1)=ymax;
        plot([trace(1,count),0],[trace(2,count),ymax],'k-','linewidth',0.6);
        plot(0,ymax,'ko','markersize',5,'markerface','k');
        count=count+1;
        r=setVariable(3*pi/2,2*pi,'normal',1);
        trace(1,count+1)=d(n)*cos(r);
        trace(2,count+1)=ymax+d(n)*sin(r);
        plot([0,trace(1,count+1)],[ymax,trace(2,count+1)],'k-','linewidth',0.6);
        count=count+1;
    elseif trace(1,count+1)<0&&trace(2,count+1)<0
        trace(1,count+1)=0;
        trace(2,count+1)=0;
        plot([trace(1,count),0],[trace(2,count),0],'k-','linewidth',0.6);
        plot(0,0,'ko','markersize',5,'markerface','k');
        count=count+1;
        r=setVariable(0,pi/2,'normal',1);
        trace(1,count+1)=d(n)*cos(r);
        trace(2,count+1)=d(n)*sin(r);
        plot([0,trace(1,count+1)],[0,trace(2,count+1)],'k-','linewidth',0.6);
        count=count+1;
    elseif trace(1,count+1)>=xmax&&trace(2,count+1)>=0&&trace(2,count+1)<=ymax
        y=((xmax-trace(1,count))*trace(2,count+1)+(trace(1,count+1)-xmax)*...
        trace(2,count))/(trace(1,count+1)-trace(1,count));
        trace(1,count+1)=xmax;
```

```
        trace(2,count+1)=y;
        plot([trace(1,count),xmax],[trace(2,count),y],'k-','linewidth',0.6);
        plot(xmax,y,'ko','markersize',5,'markerface','k');
        count=count+1;
        r=setVariable(pi/2,3*pi/2,'normal',1);
        trace(1,count+1)=xmax+d(n)*cos(r);
        trace(2,count+1)=y+d(n)*sin(r);
        plot([xmax,trace(1,count+1)],[y,trace(2,count+1)],'k-','linewidth',0.6);
        count=count+1;
    elseif trace(1,count+1)<=0&&trace(2,count+1)>=0&&trace(2,count+1)<=ymax
        y=((0-trace(1,count))*trace(2,count+1)+trace(1,count+1)*...
        trace(2,count))/(trace(1,count+1)-trace(1,count));
        trace(1,count+1)=0;
        trace(2,count+1)=y;
        plot([trace(1,n),0],[trace(2,n),y],'k-','linewidth',0.6);
        plot(0,y,'ko','markersize',5,'markerface','k');
        count=count+1;
        r=setVariable(3*pi/2,5*pi/2,'normal',1);
        trace(1,count+1)=d(n)*cos(r);
        trace(2,count+1)=y+d(n)*sin(r);
        plot([0,trace(1,count+1)],[y,trace(2,count+1)],'k-','linewidth',0.6);
        count=count+1;
    elseif trace(2,count+1)>=ymax&&trace(1,count+1)>=0&&trace(1,count+1)<=xmax
        x=((ymax-trace(2,count))*trace(1,count+1)+(trace(2,count+1)-ymax)*...
        trace(1,count))/(trace(2,count+1)-trace(2,count));
        trace(1,count+1)=x;
        trace(2,count+1)=ymax;
        plot([trace(1,count),x],[trace(2,count),ymax],'k-','linewidth',0.6);
        plot(x,ymax,'ko','markersize',5,'markerface','k');
        count=count+1;
        r=setVariable(pi,2*pi,'normal',1);
        trace(1,count+1)=x+d(n)*cos(r);
        trace(2,count+1)=ymax+d(n)*sin(r);
        plot([x,trace(1,count+1)],[ymax,trace(2,count+1)],'k-','linewidth',0.6);
        count=count+1;
    elseif trace(2,count+1)<=0&&trace(1,count+1)>=0&&trace(1,count+1)<=xmax
        x=((0-trace(2,count))*trace(1,count+1)+trace(2,count+1)*...
        trace(1,count))/(trace(2,count+1)-trace(2,count));
        trace(1,count+1)=x;
```

```
        trace(2,count+1)=0;
        plot([trace(1,count),x],[trace(2,count),0],'k-','linewidth',0.6);
        plot(x,0,'ko','markersize',5,'markerface','k');
        count=count+1;
        r=setVariable(0,pi,'normal',1);
        trace(1,count+1)=x+d(n)*cos(r);
        trace(2,count+1)=d(n)*sin(r);
        h3=plot([x,trace(1,count+1)],[0,trace(2,count+1)],'k-','linewidth',0.6);
        count=count+1;
    end
    drawnow;
end

% ending point
h2=plot(trace(1,end),trace(2,end),'ro','markersize',10,'linewidth',1.5);

legend([h1,h2,h3,h4],'starting point','terminal point','track','boundary');
xlabel('x [m]');
ylabel('y [m]');

hold off;
%title(['Random Direction Mobility Mode','total ',num2str(N),' moves']);
%}

%{
%% 3-D
trace(3,:) = thirdDi(length(trace(1,:))-1,t,z0,zmin,zmax);
%%}

trace_rss=trace;

save('random_direction_25.mat');
%}
```

APPENDIX B. HYBRID MODEL SIMULATOR

```
%%%%%%%%%%%%%%%%%%%%%%%%%%%%%%%%%%%%%%%%%%%%%%%%%%%%%%%%%%%%%%%%%%%%%%%%%%%%
%                                                                             %
%       Department of Electronics and Communication Engineering               %
%                          WANG WENBO - 238970                                %
%                                                                             %
%                           hybrid model - 3D                                 %
%                                                                             %
%%%%%%%%%%%%%%%%%%%%%%%%%%%%%%%%%%%%%%%%%%%%%%%%%%%%%%%%%%%%%%%%%%%%%%%%%%%%

close all;
clear all;
clc;

%%%%%%%%%%%%%%%%%%%%%%%%%%%%%%%%%%%%%%%%%%%%%%%%%%%%%%%%%%%%%%%%%%%%%%%%%%%%
% Explanation                                                                 %
%In this model, the random direction mobility model and random waypoint      %
%mobility model are combined, so that it starts moving from (an random       %
%point in the area), and with (a certain direction and changing velocity%
%), maintaining this status for (a while), before or touching the            %
%boundry, changing direction and repeat this action again.                   %
%    Note :                                                                  %
% in this model, the normal distribution is used with confident level        %
%95% to model velocity and angles.                                           %
%%%%%%%%%%%%%%%%%%%%%%%%%%%%%%%%%%%%%%%%%%%%%%%%%%%%%%%%%%%%%%%%%%%%%%%%%%%%


%% variable
% define x-y plane
xmax=50;ymax=50;

% the number of floors
noOfFloor=3;

% the height spacing of floors
floorHeight=3;
```

```
% simulation times (pause also counted as 1 time simulation)
n=10000;
n=2*ceil(n/2);

% define the upper and lower bound of velocity [m/s]
v_min=0.5;v_max=3;
%v_min=0.89;v_max=1.083;

% define the upper and lower bound of angle [radian]
r_min=0;r_max=2*pi;

% define the move time bound [s]
t_move_min=3;t_move_max=10;

% define the pause time bound [s]
t_pause_min=0.5;t_pause_max=30;

% define the upper and lower bound of distance away from boundry [m]
dist_min=0.5;dist_max=20;

%% avariable models using setVariable function
v=setVariable(v_min,v_max,'normal',n/2);
r=setVariable(r_min,r_max,'uniform',n/2);
t_m=setVariable(t_move_min,t_move_max,'normal',n/2);
t_p=setVariable(t_pause_min,t_pause_max,'normal',n/2);
dist=setVariable(dist_min,dist_max,'uniform',n);

% define the total simulation time [s]
% the first row is move time, second row is pause time
t(1,:)=t_m;
t(2,:)=t_p;

% define the sampling frequency [Hz]
Fs=1e2;

% define the starting point x-y-z
temp_3=0:floorHeight:floorHeight*(noOfFloor-1);
%startP=[0,0,0];
```

```
%startP=[xmax*rand,ymax*rand,temp_3(randi(length(temp_3)))];
load('para3.mat');

%% process

% initial

t=floor(t*Fs);
t=[zeros(2,1),t];

trace(1:3,1)=startP;

counta=1;% for angle purpose
countb=1;% for dist purpose

for p=1:n/2

    count1=sum(t(1,1:p))+1;
    count2=sum(t(1,1:p+1));

    ang=r(counta);

    for pp=count1:count2

        trace(1,pp+1)=trace(1,pp)+v(p)*cos(ang)/Fs;
        trace(2,pp+1)=trace(2,pp)+v(p)*sin(ang)/Fs;
        temp_3=thirdDi(1,1/Fs,trace(3,pp),0,(noOfFloor-1)*floorHeight);
        trace(3,pp+1)=temp_3(2);

        temp1=trace(1,pp+1)+dist(countb);
        temp2=trace(2,pp+1)+dist(countb);
        temp3=trace(1,pp+1)-dist(countb);
        temp4=trace(2,pp+1)-dist(countb);

        if temp1<xmax&&temp3>0&&temp2<ymax&&temp4>0
            continue;
        elseif temp1>xmax&&temp4<0
            ang=setVariable(pi/2,pi,'normal',1);
            trace(1,pp+1)=trace(1,pp)+v(p)*cos(ang)/Fs;
```

```
            trace(2,pp+1)=trace(2,pp)+v(p)*sin(ang)/Fs;
        elseif temp1>xmax&&temp2>ymax
            ang=setVariable(pi,3*pi/2,'normal',1);
            trace(1,pp+1)=trace(1,pp)+v(p)*cos(ang)/Fs;
            trace(2,pp+1)=trace(2,pp)+v(p)*sin(ang)/Fs;
        elseif temp3<0&&temp2>ymax
            ang=setVariable(3*pi/2,2*pi,'normal',1);
            trace(1,pp+1)=trace(1,pp)+v(p)*cos(ang)/Fs;
            trace(2,pp+1)=trace(2,pp)+v(p)*sin(ang)/Fs;
        elseif temp3<0&&temp4<0
            ang=setVariable(0,pi/2,'normal',1);
            trace(1,pp+1)=trace(1,pp)+v(p)*cos(ang)/Fs;
            trace(2,pp+1)=trace(2,pp)+v(p)*sin(ang)/Fs;
        elseif temp1>=xmax&&temp4>=0&&temp2<=ymax
            ang=setVariable(pi/2,3*pi/2,'normal',1);
            trace(1,pp+1)=trace(1,pp)+v(p)*cos(ang)/Fs;
            trace(2,pp+1)=trace(2,pp)+v(p)*sin(ang)/Fs;
        elseif temp3<=0&&temp4>=0&&temp2<=ymax
            ang=setVariable(3*pi/2,5*pi/2,'normal',1);
            trace(1,pp+1)=trace(1,pp)+v(p)*cos(ang)/Fs;
            trace(2,pp+1)=trace(2,pp)+v(p)*sin(ang)/Fs;
        elseif temp2>=ymax&&temp3>=0&&temp1<=xmax
            ang=setVariable(pi,2*pi,'normal',1);
            trace(1,pp+1)=trace(1,pp)+v(p)*cos(ang)/Fs;
            trace(2,pp+1)=trace(2,pp)+v(p)*sin(ang)/Fs;
        elseif temp4<=0&&temp3>=0&&temp1<=xmax
            ang=setVariable(0,pi,'normal',1);
            trace(1,pp+1)=trace(1,pp)+v(p)*cos(ang)/Fs;
            trace(2,pp+1)=trace(2,pp)+v(p)*sin(ang)/Fs;
        end

    end

    counta=counta+1;
    countb=countb+1;

end

tm=floor(t_m*Fs);
```

```
tp=floor(t_p*Fs);

for ppp=1:n/2

    trace_rss(1,1+sum(tm(1:ppp-1))+sum(tp(1:ppp-1)):1+sum(tm(1:ppp))...
    +sum(tp(1:ppp-1)))=trace(1,1+sum(tm(1:ppp-1)):1+sum(tm(1:ppp)));
    trace_rss(1,2+sum(tm(1:ppp))+sum(tp(1:ppp))-tp(ppp):1+sum(tm(1:ppp))...
    +sum(tp(1:ppp)))=trace(1,1+sum(tm(1:ppp)));
    trace_rss(2,1+sum(tm(1:ppp-1))+sum(tp(1:ppp-1)):1+sum(tm(1:ppp))...
    +sum(tp(1:ppp-1)))=trace(2,1+sum(tm(1:ppp-1)):1+sum(tm(1:ppp)));
    trace_rss(2,2+sum(tm(1:ppp))+sum(tp(1:ppp))-tp(ppp):1+sum(tm(1:ppp))...
    +sum(tp(1:ppp)))=trace(2,1+sum(tm(1:ppp)));
    trace_rss(3,1+sum(tm(1:ppp-1))+sum(tp(1:ppp-1)):1+sum(tm(1:ppp))...
    +sum(tp(1:ppp-1)))=trace(3,1+sum(tm(1:ppp-1)):1+sum(tm(1:ppp)));
    trace_rss(3,2+sum(tm(1:ppp))+sum(tp(1:ppp))-tp(ppp):1+sum(tm(1:ppp))...
    +sum(tp(1:ppp)))=trace(3,1+sum(tm(1:ppp)));

end

%save('hybrid_model_2_35.mat');
```